Optimal Spectral Decomposition (OSD) for Ocean Data Analysis

Peter C Chu[1] and Charles Sun[2]

[1] Naval Postgraduate School, Monterey, CA 93943

pcchu@nps.edu, http://faculty.nps.edu/pcchu/

[2] NOAA/NODC, Silver Spring, MD 20910

Charles.Sun@noaa.gov

GTSPP Meeting, Honolulu, Hawaii, 27 October 2008

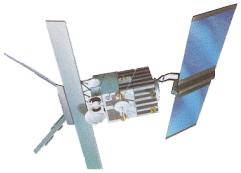

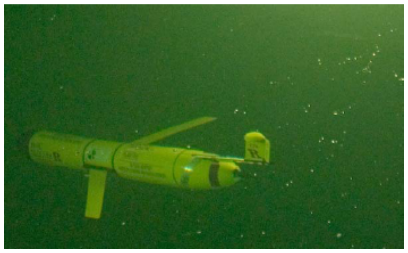

w can we effectively use observational ocean
ta to represent and to predict the ocean state

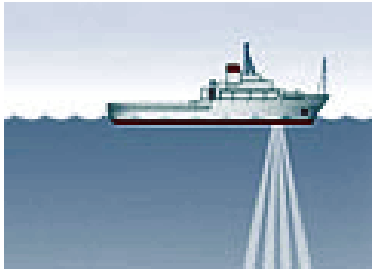

Collaborators

- Leonid M. Ivanov (California State Univ)
- Chenwu Fan (NPS)
- Tateana Margolina (NPS)
- Oleg Melnichenko (Univ of Hawaii)

References

- Chu, P.C., L.M. Ivanov, T.P. Korzhova, T.M. Margolina, and O.M. Melnichenko, 2003a: Analysis of sparse and noisy ocean current data using flow decomposition. Part 1: Theory. Journal of Atmospheric and Oceanic Technology, 20 (4), 478-491.

- Chu, P.C., L.M. Ivanov, T.P. Korzhova, T.M. Margolina, and O.M. Melnichenko, 2003b: Analysis of sparse and noisy ocean current data using flow decomposition. Part 2: Application to Eulerian and Lagrangian data. Journal of Atmospheric and Oceanic Technology, 20 (4), 492-512.

- Chu, P.C., L.M. Ivanov, and T.M. Margolina, 2004: Rotation method for reconstructing process and field from imperfect data. International Journal of Bifurcation and Chaos, 14 (04), 2991-2997.

References

- Chu, P.C., L.M. Ivanov, and T.M. Margolina, 2005: Seasonal variability of the Black Sea Chlorophyll-a concentration. Journal of Marine Systems, 56, 243-261.

- Chu, P.C., L.M. Ivanov, and O.M. Melnichenko, 2005: Fall-winter current reversals on the Texas-Lousiana continental shelf. Journal of Physical Oceanography, 35, 902-910.

- Chu, P.C., L.M. Ivanov, O.V. Melnichenko, and N.C. Wells, 2007: On long baroclinic Rossby waves in the tropical North Atlantic observed from profiling floats. Journal of Geophysical Research, 112, C05032, doi:10.1029/2006JC003698.

- Chu, P. C., L. M. Ivanov, O. V. Melnichenko, and R.-F. Li, 2008: Argo floats revealing bimodality of large-scale mid-depth circulation in the North Atlantic. Acta Oceanologica Sinica, 27 (2), 1-10.

- Chu, P.C., C. Sun, and C. Fan, 2009: Variability in meridional overturning circulation and thermohaline structure detected from GTSPP/Argo/MOODS/OSCAR Data. Proceedings on 21th Symposium on Climate Variability, American Meteorological Society, Phoenix, January 11-15, 2009.

Observational Data

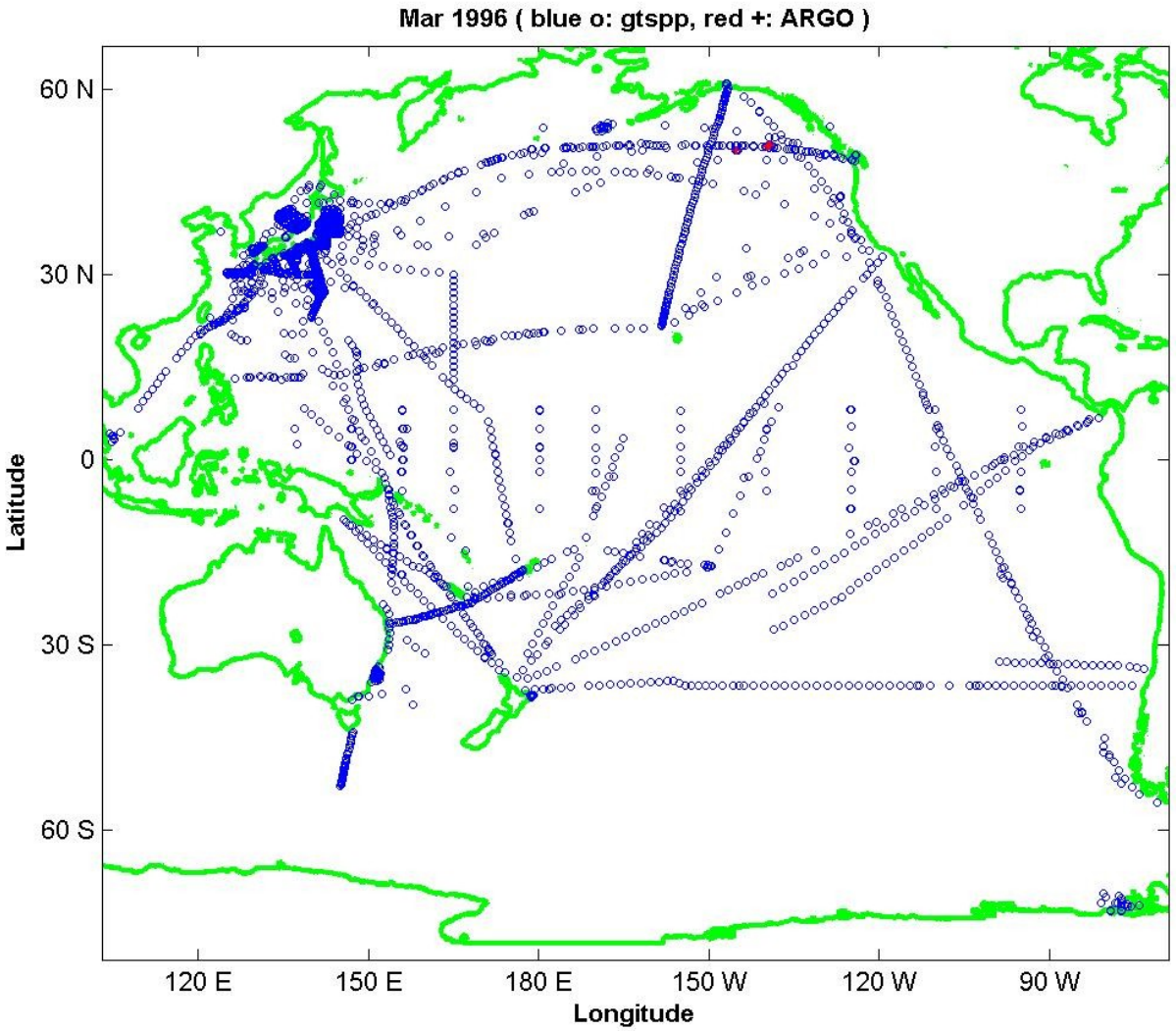

A Popular Method for Ocean Data Analysis: Optimum Interpolation (OI)

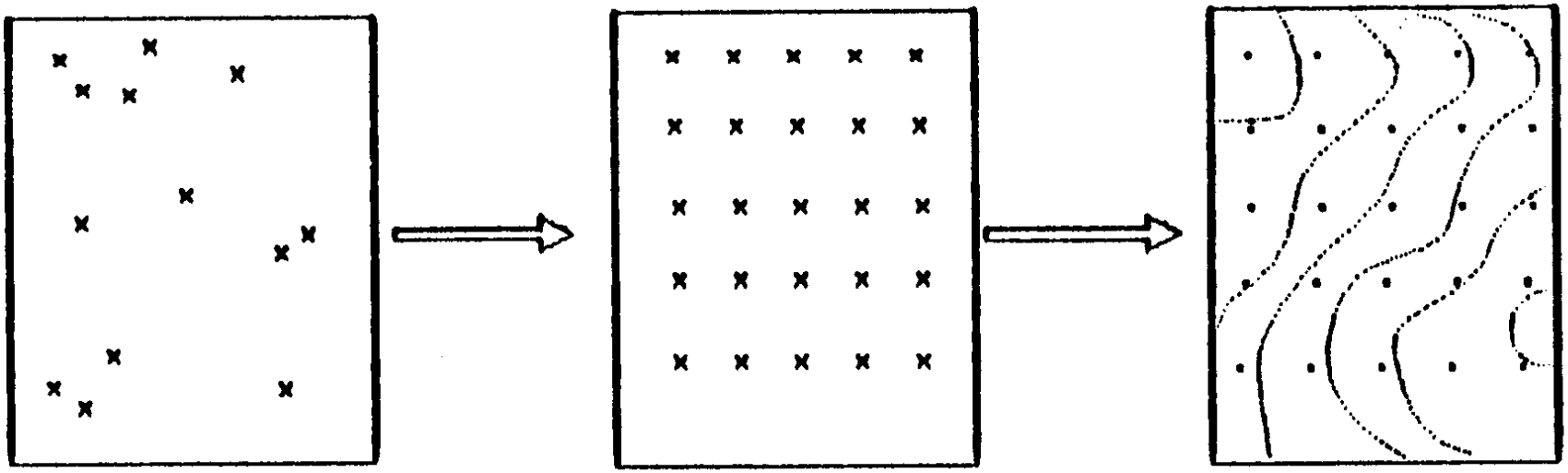

OI – Equation

Grid point → k, Observational Point → j

Q_k^f → First guess field (gridded)

Q_j^o → Observation

Q_j^f → First guess interpolated on the observational point

$$Q_k^a = Q_k^f + \sum_{j=1}^{N} a_{kj}(Q_j^o - Q_j^f)$$

Q_k^a → Analyzed field at the grid point

OI – Weight Coefficients a_{kj}

$$\sum_{j=1}^{N} (h_{ij} + d_{ij} I_i^o) a_{kj} = h_{kj}$$

h_{ij} h_{kj} → Autocorrelation functions

I_i^o → Signal-to-noise ratio

Three Requirements for the OI Method

- (1) First guess field
- (2) Autocorrelation functions
- (3) High signal-to-noise ratio

What happens if the three conditions are not satisfied?

Spectral Representation - a Possible Alternative Method

$$c(\mathbf{x}, z_k, t) = A_0(z_k, t) + \sum_{m=1}^{M} A_m(z_k, t)\ \Psi_m(\mathbf{x}, z_k),$$

Ψ_m → Basis functions

c → any ocean variable

Flow Decomposition

$$u = \frac{\partial \Psi}{\partial y} + \frac{\partial^2 \Phi}{\partial x \partial z}, \qquad v = -\frac{\partial \Psi}{\partial x} + \frac{\partial^2 \Phi}{\partial y \partial z},$$

$$\triangle \Psi = -\zeta$$

$$\triangle \Phi = -w$$

Basis Functions (Closed Basin)

$$\triangle \Psi_k = -\lambda_k \Psi_k, \quad \Psi_k|_\Gamma = 0, \qquad k = 1, ..., \infty$$

$$\triangle \Phi_m = -\mu_m \Phi_m, \quad \frac{\partial \Phi_m}{\partial n}|_\Gamma = 0, \qquad m = 1, ..., \infty.$$

Basis Functions (Open Boundaries)

$$\triangle \Psi_k = -\lambda_k \Psi_k,$$

$$\triangle \Phi_m = -\mu_m \Phi_m,$$

$$\Psi_k|_\Gamma = 0, \quad \frac{\partial \Phi_m}{\partial n}|_\Gamma = 0,$$

$$\left[\frac{\partial \Psi_k}{\partial n} + \kappa(\tau)\Psi_k\right]|_{\Gamma_1'} = 0, \quad \Phi_m|_{\Gamma_1'} = 0,$$

Boundary Conditions

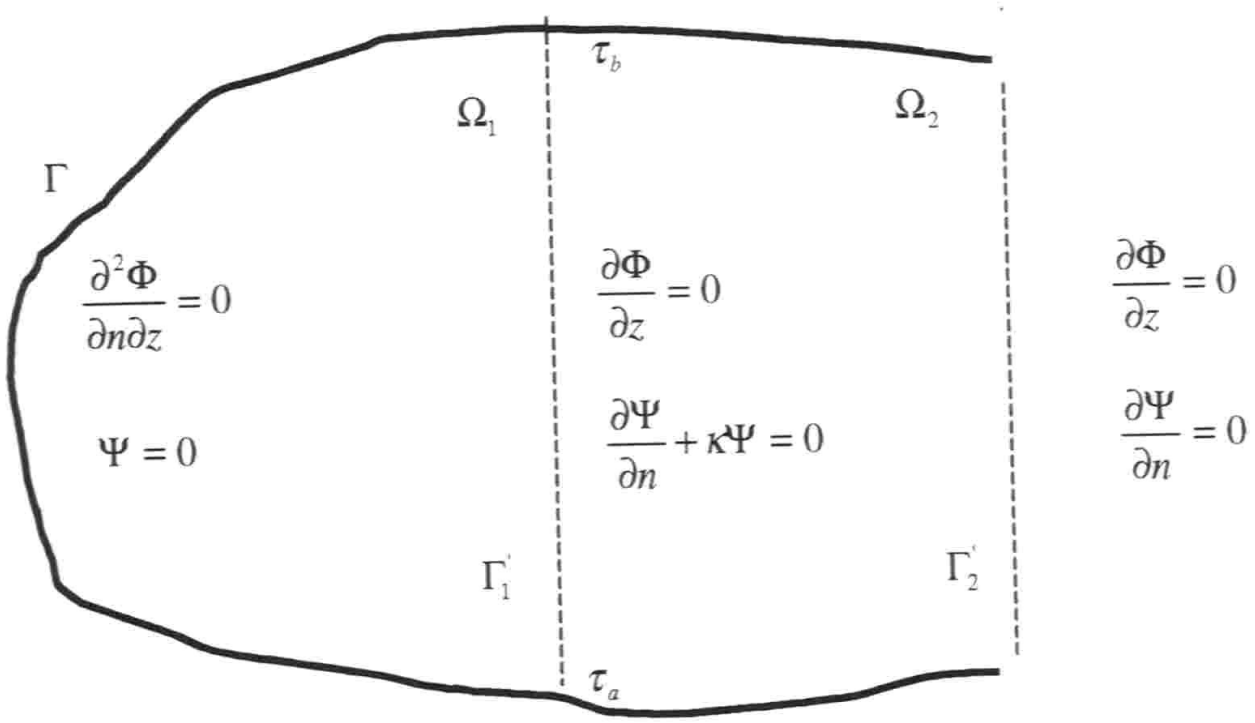

Spectral Decomposition

$$u_{KM} = \sum_{k=1}^{K} a_k(z,t^\circ)\frac{\partial \Psi_k(x,y,z,\kappa^\circ)}{\partial y} + \sum_{m=1}^{M} b_m(z,t^\circ)\frac{\partial \Phi_m(x,y,z)}{\partial x},$$

$$v_{KM} = -\sum_{k=1}^{K} a_k(z,t^\circ)\frac{\partial \Psi_k(x,y,z,\kappa^\circ)}{\partial x} + \sum_{m=1}^{M} b_m(z,t^\circ)\frac{\partial \Phi_m(x,y,z)}{\partial y}$$

$$T(\mathbf{x},t) = T_0(\mathbf{x}) + \sum_{m=1}^{M} c_m(t)\mathrm{F}_m(\mathbf{x},t)$$

$$S(\mathbf{x},t) = S_0(\mathbf{x}) + \sum_{m=1}^{M} d_m(t)\mathrm{F}_m(\mathbf{x},t)$$

Benefits of Using OSD

- (1) Don’t need first guess field
- (2) Don’t need autocorrelation functions
- (3) Don’t require high signal-to-noise ratio
- (4) Basis functions are pre-determined before the data analysis.

Optimal Mode Truncation

$$J(a_{1,\dots,}a_K, b_{1,\dots,}b_M, \kappa, P) = \frac{1}{2}\left(\left\|u_p^{obs} - u_{KM}\right\|_P^2 + \left\|v_p^{obs} - v_{KM}\right\|_P^2\right) \to \min,$$

Vapnik (1983) Cost Function

$$J_{emp} = J(a_{1,\ldots,}a_K, b_{1,\ldots,}b_M, \kappa, P).$$

$$\text{Prob}\left\{ \sup_{K,M,S} |\langle J(K,M,S)\rangle - J_{emp}(K,M,S)| \geq \mu \right\} \leq g(P,\mu)$$

$$\lim_{P\to\infty} g(P,\mu) = 0$$

Optimal Truncation

- Gulf of Mexico, Monterey Bay, Louisiana-Texas Shelf, North Atlantic

- $K_{opt} = 40$, $M_{opt} = 30$

Determination of Spectral Coefficients (Ill-Posed Algebraic Equation)

$$\mathbf{A}\hat{\mathbf{a}} = \mathbf{QY},$$

This is caused by the features of the matrix **A**.

Rotation Method (Chu et al., 2004)

$$\mathbf{SA}\,\hat{\mathbf{a}} = \mathbf{SQY},$$

$$J_1 = \|\mathbf{A}\|^2 - \frac{\|\mathbf{SQY}\|^2}{\|\mathbf{a}\|^2} \rightarrow \max,$$

Example-1

Temporal and spatial variability of Pacific Ocean

T (10 m) 1990-2008

T (100 m) 1990-2008

T (500 m) 1990-2008

T: NINO-3 (5°S-5°N, 150°W-90°W)

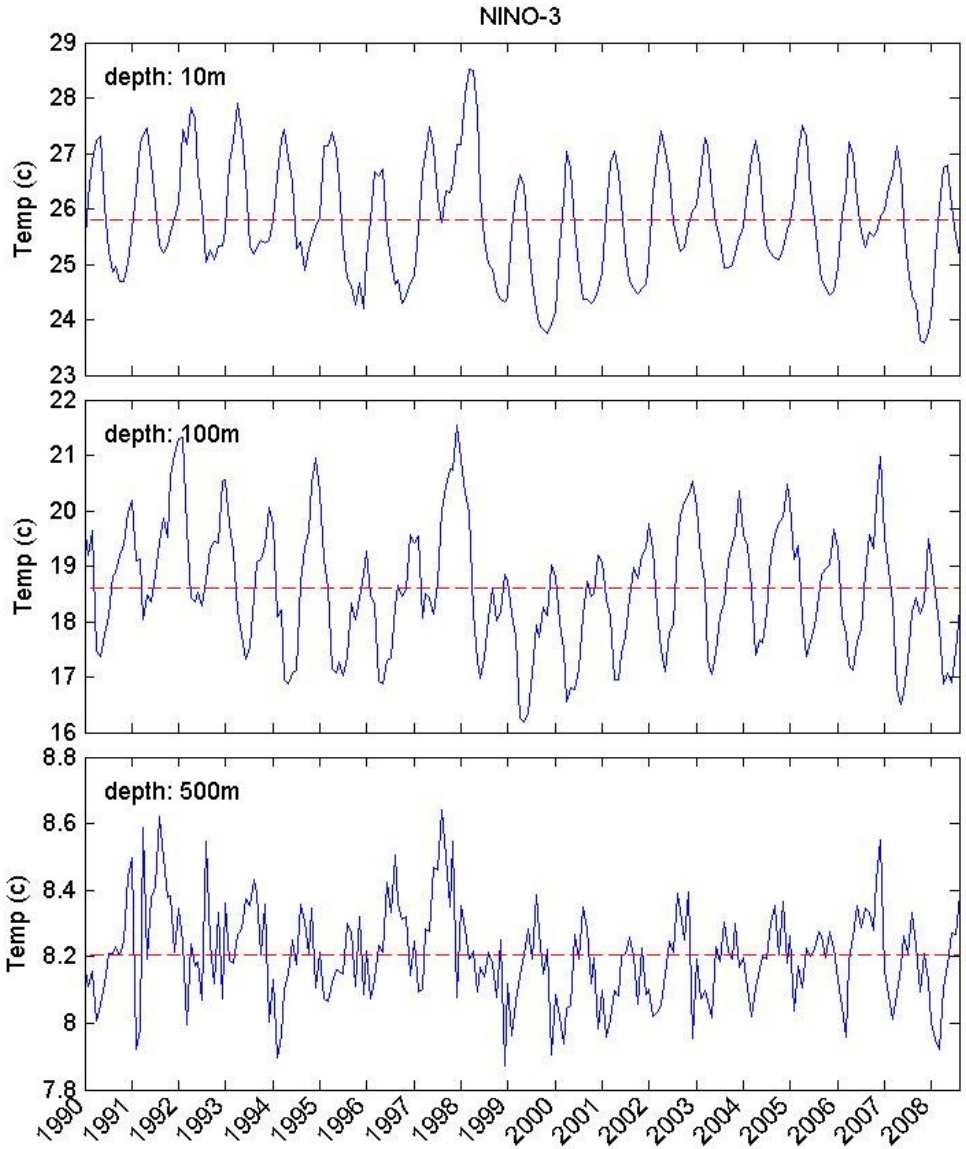

Example-2 OSD for Analyzing ARGO Data

Baroclinic Rossby Waves in the tropical North Atlantic

Tropical North Atlantic (4°-24°N)
Important Transition Zone →
Meridional Overturning Circulation
(MOC)

(Rahmstorf 2006)

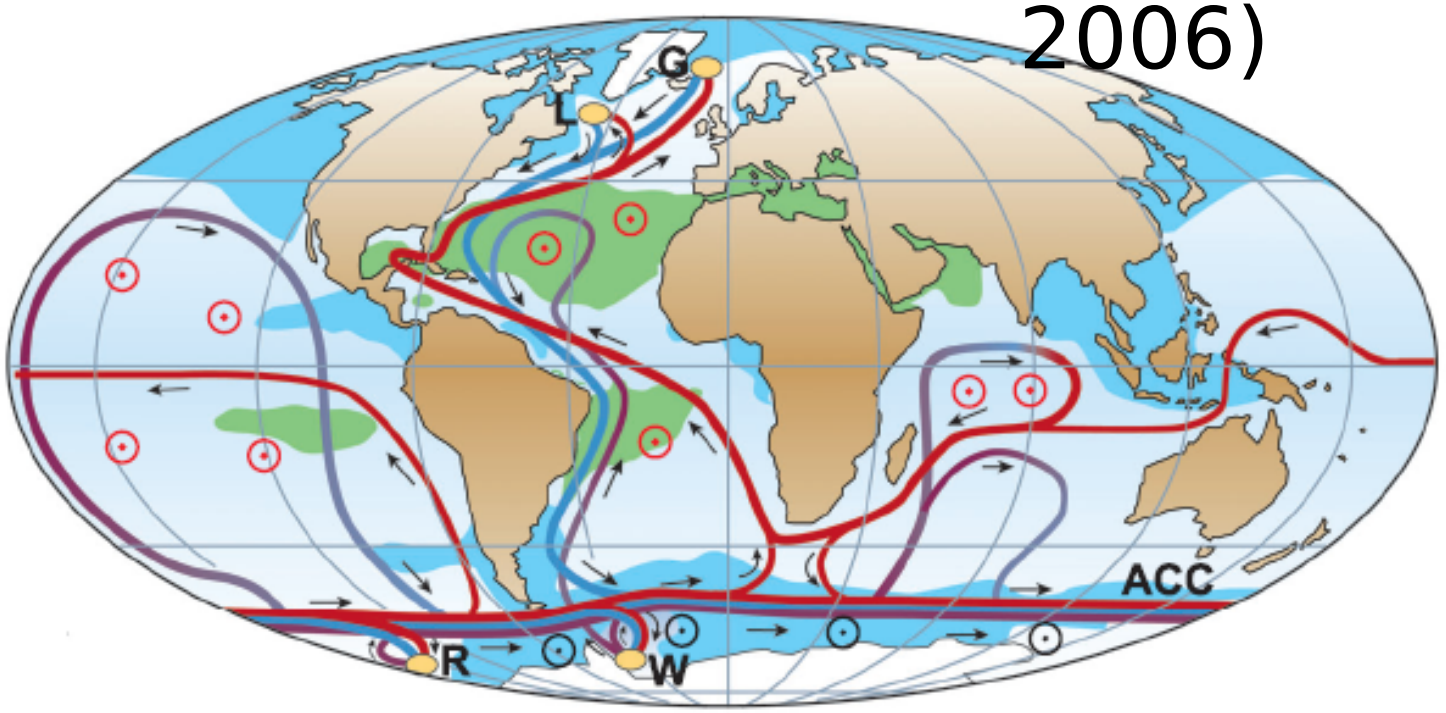

MOC Variation →

Heat Transport Variation →

Climate Change

- Are mid-depth (~1000 m) ocean circulations steady?

- If not, what mechanisms cause the change? (Rossby wave propagation)

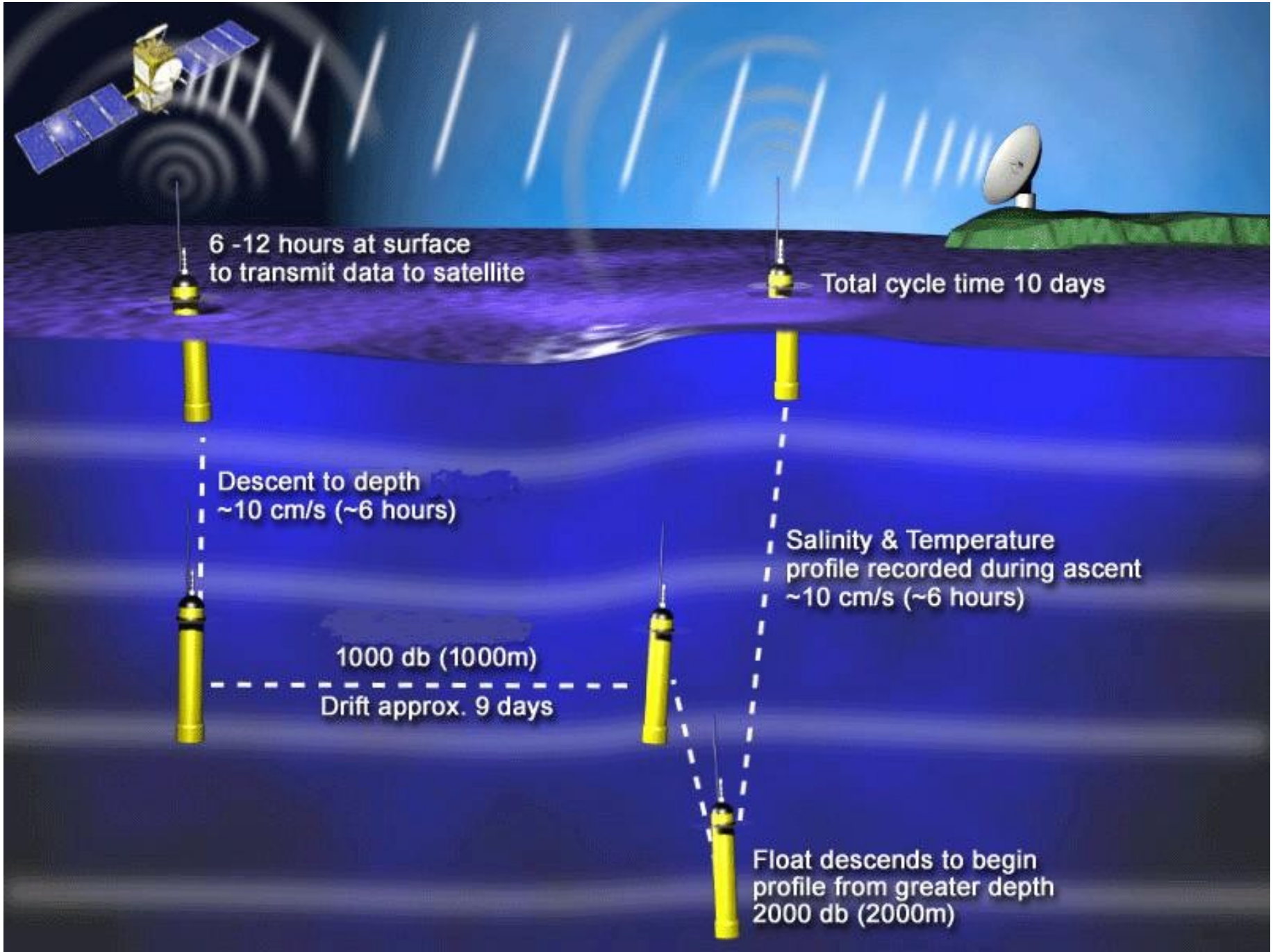
6 -12 hours at surface
to transmit data to satellite
Total cycle time 10 days
Descent to depth
~10 cm/s (~6 hours)
Salinity & Temperature
profile recorded during ascent
~10 cm/s (~6 hours)
1000 db (1000m)
Drift approx. 9 days
Float descends to begin
profile from greater depth
2000 db (2000m)

ARGO Observations (Oct-Nov 2004)

(a) Subsurface tracks

(b) Float positions where (T,S) were measured

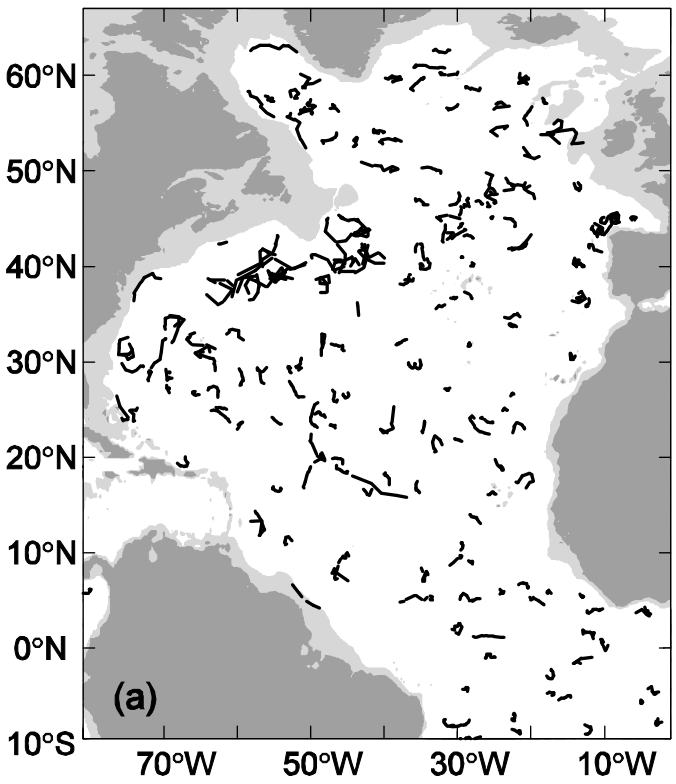

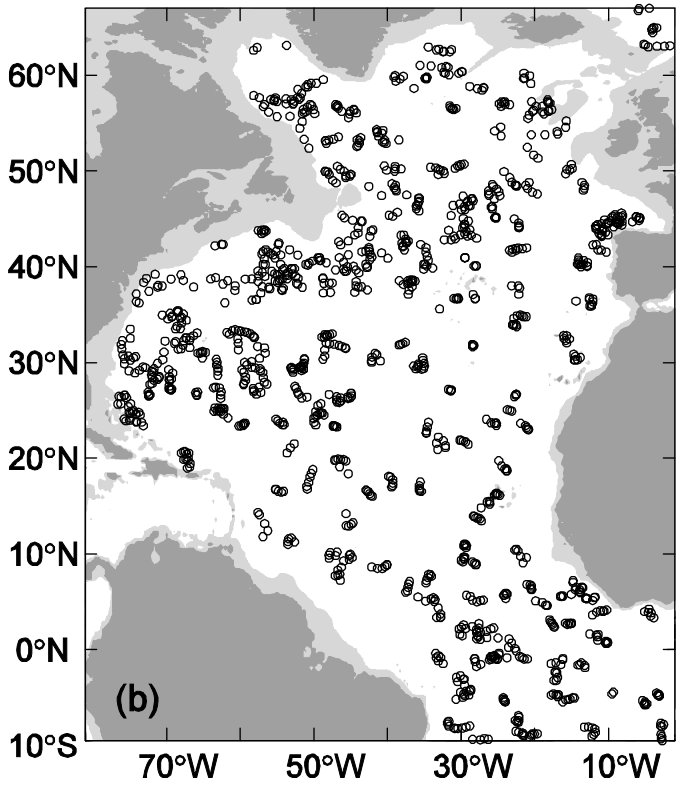

Circulations at 1000 m estimated from the original ARGO float tracks (bin method) April 2004 – April 2005

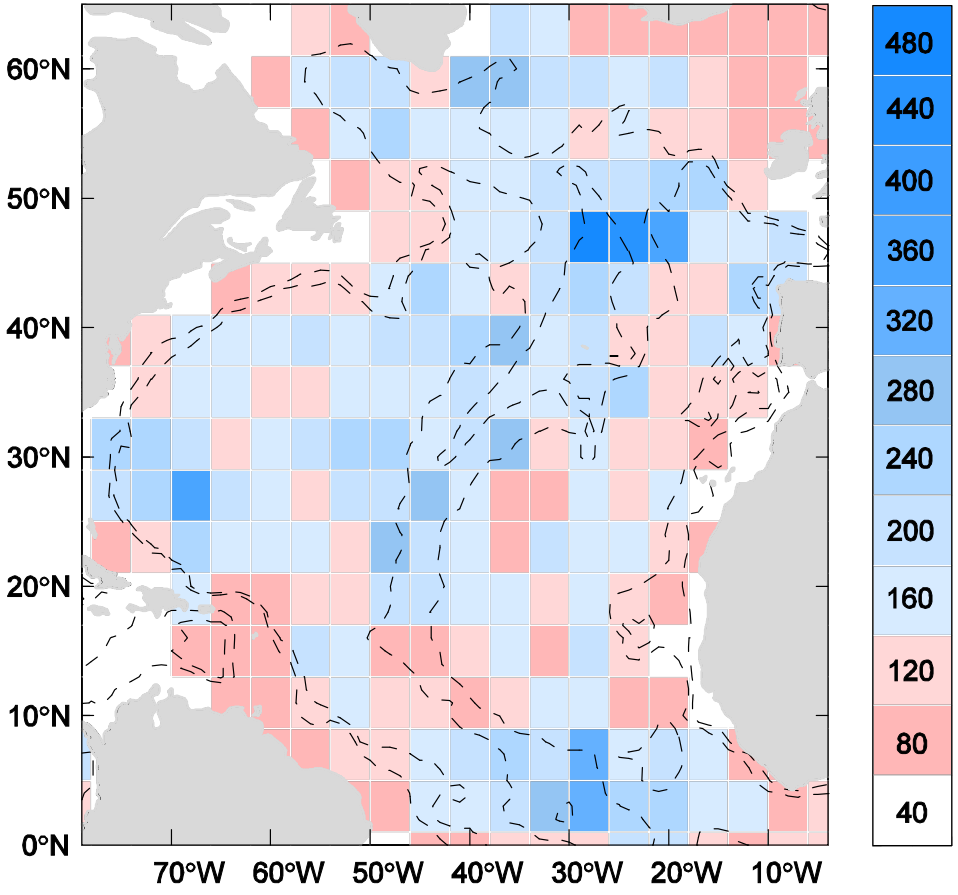

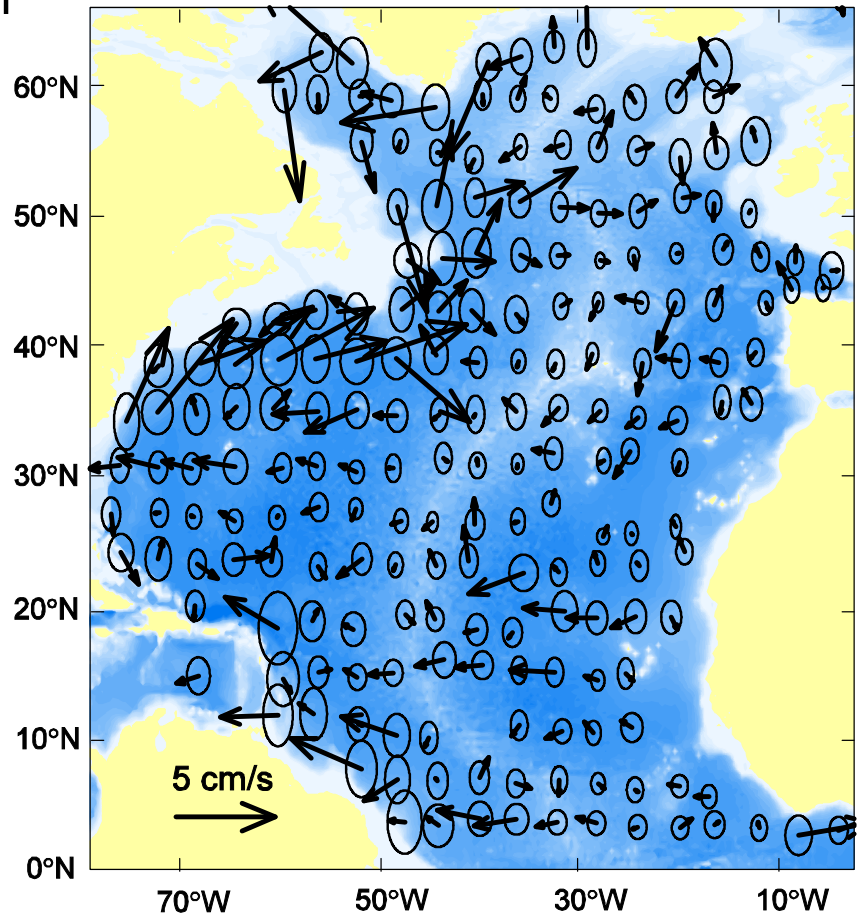

is difficult to get physical insights and
o use such noisy data into ocean numerical models.

Boundary Configuration → Basis Functions for OSD

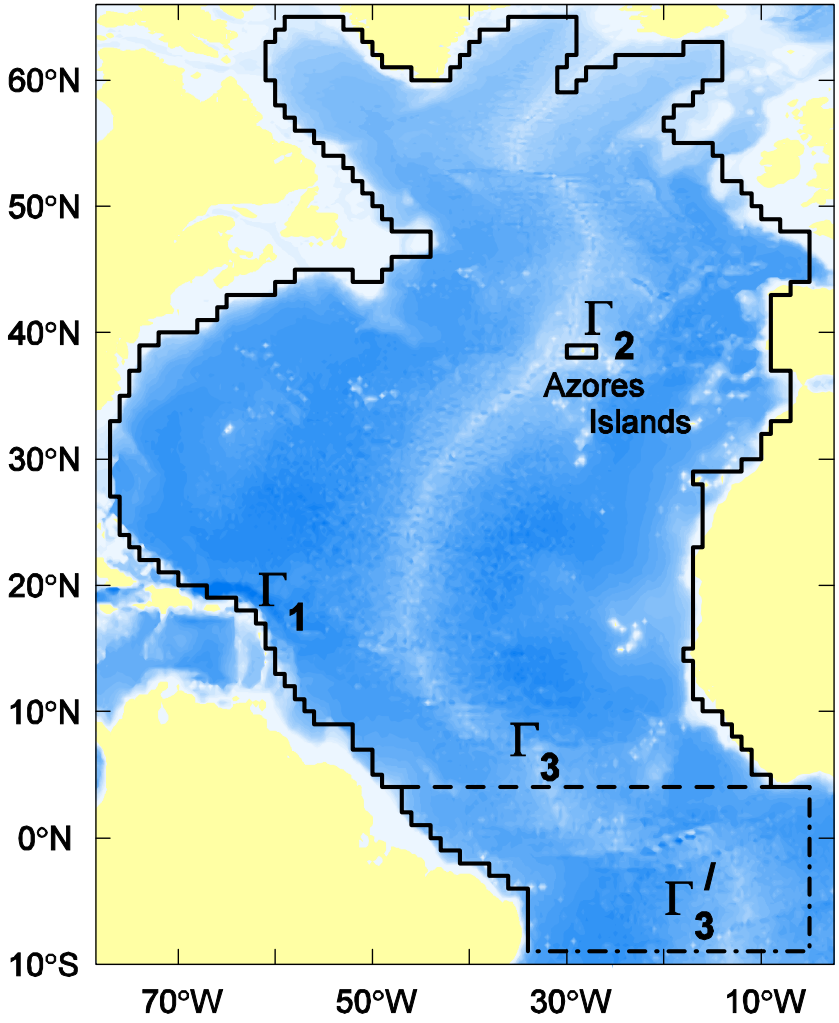

Basis Functions for Streamfunction Mode-1 and Mode-2

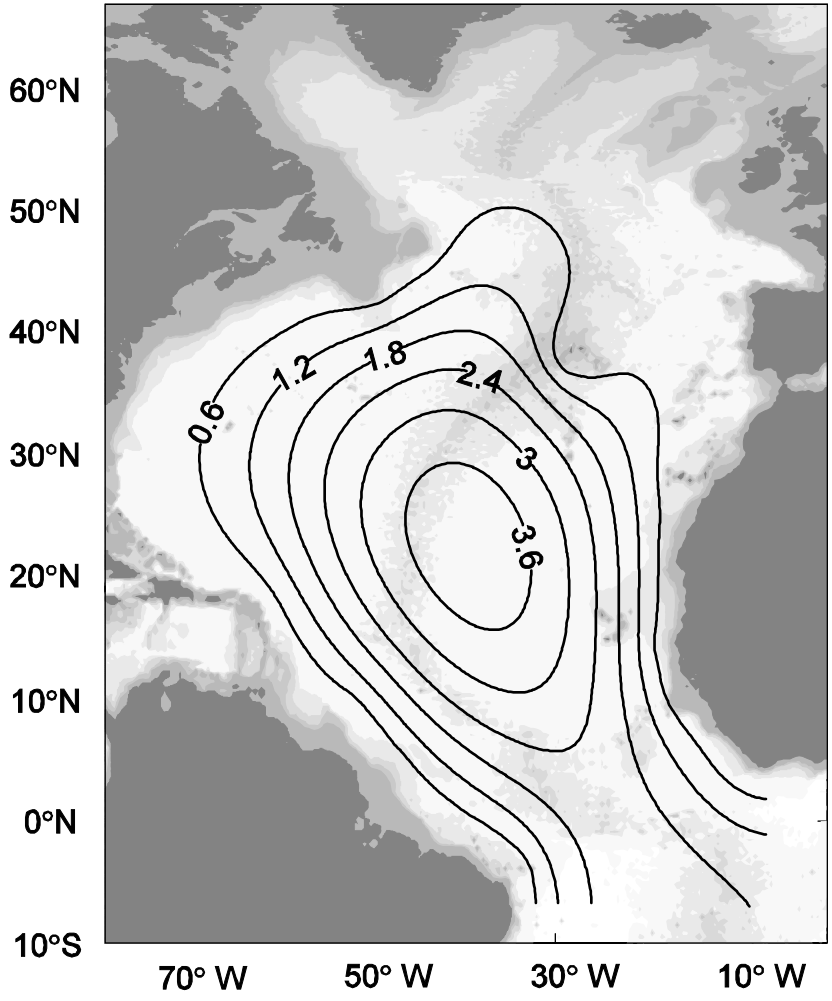

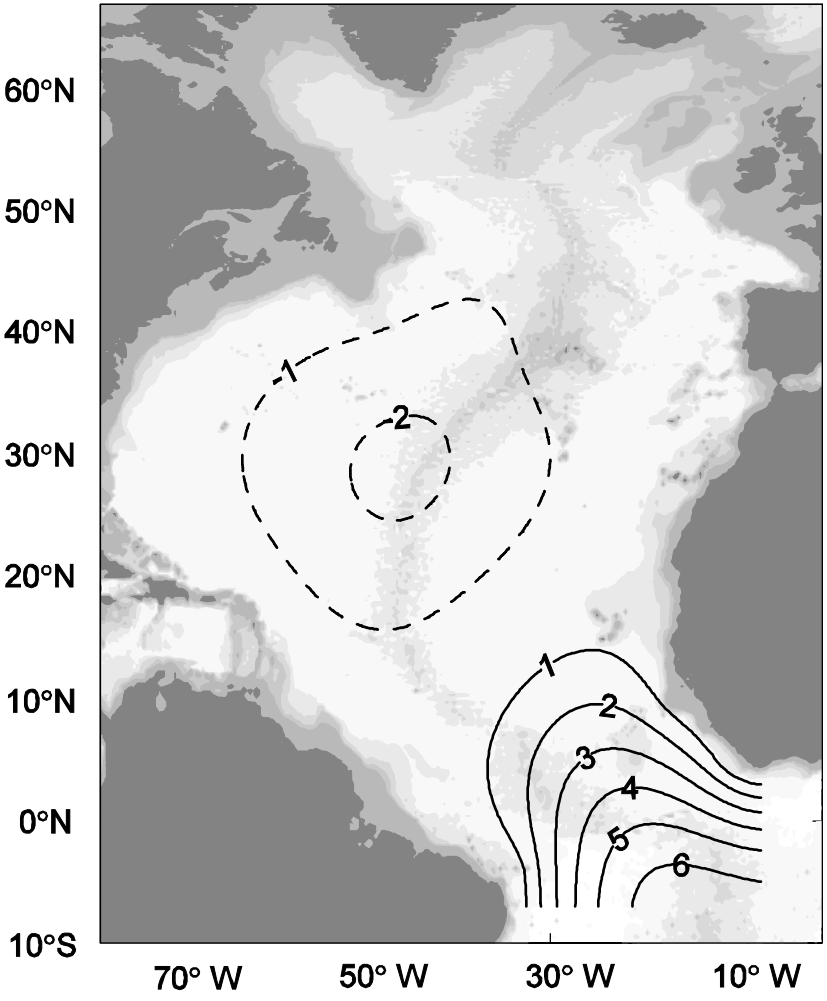

Circulations at 1000 m (March 04 to May 05)

Bin Method

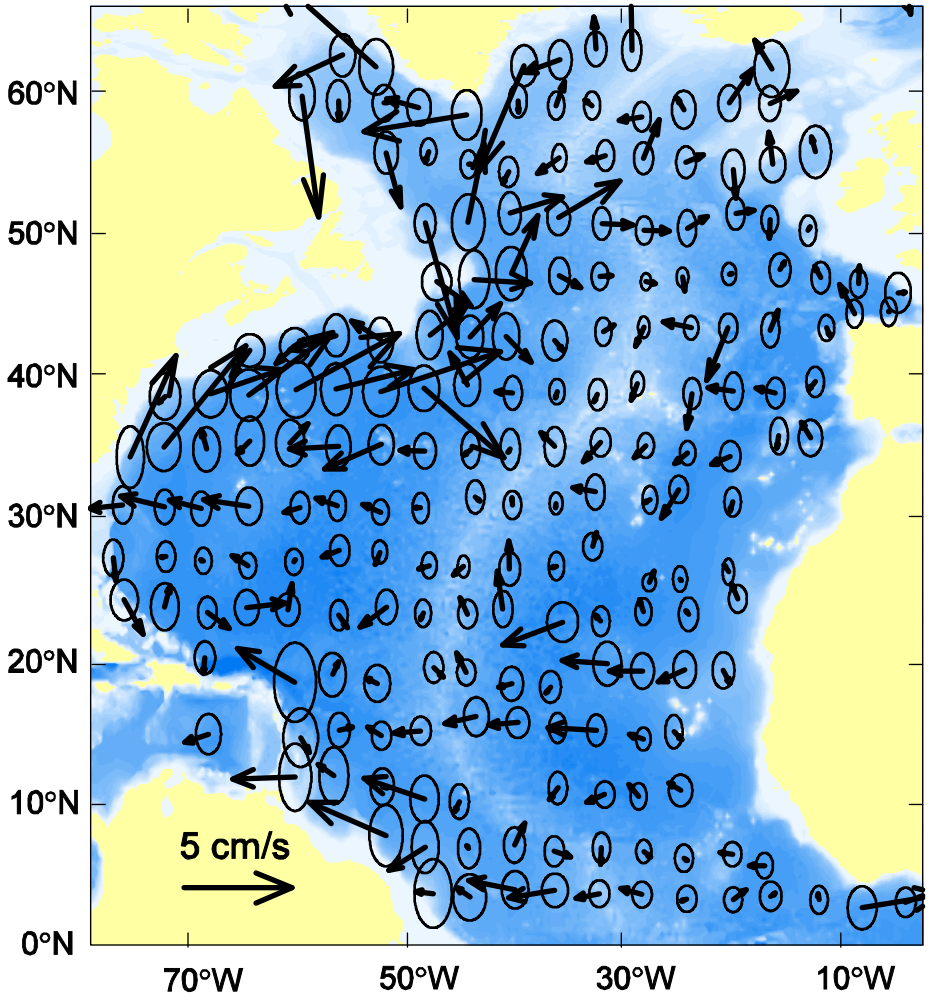

OSD

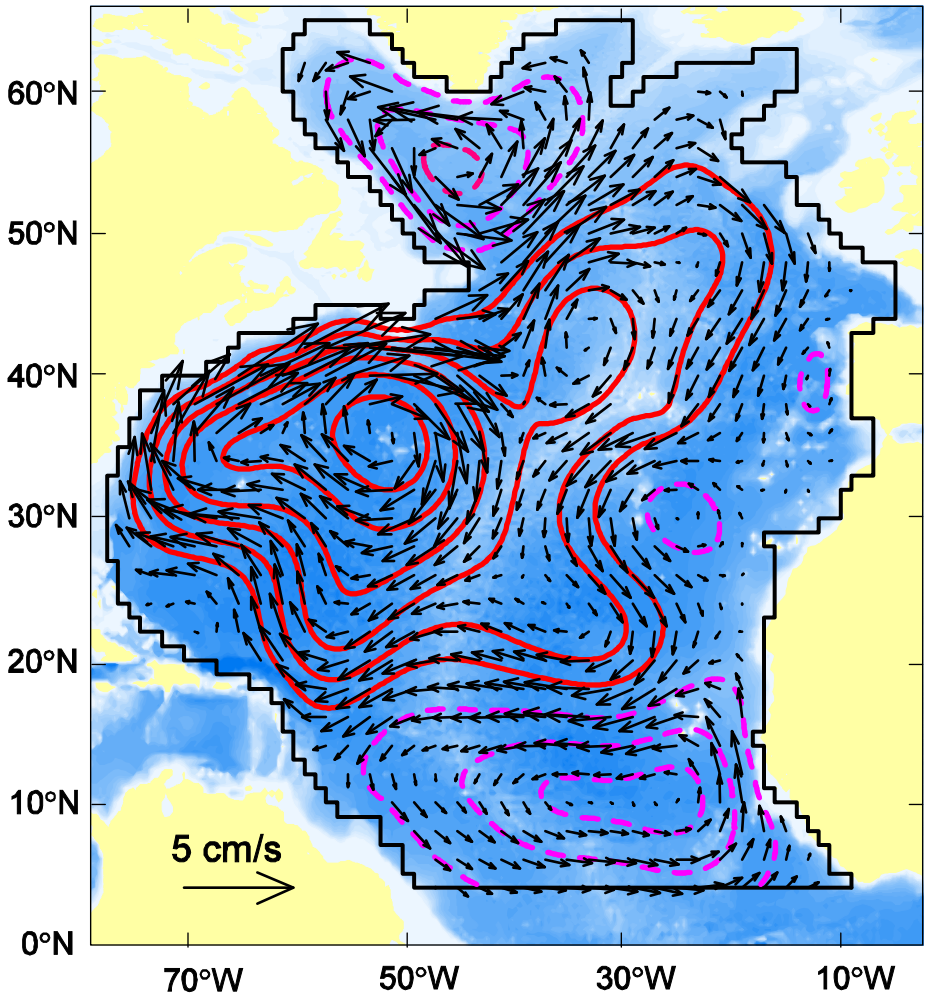

Mid-Depth Circulations (1000 m)

Mar-May 04

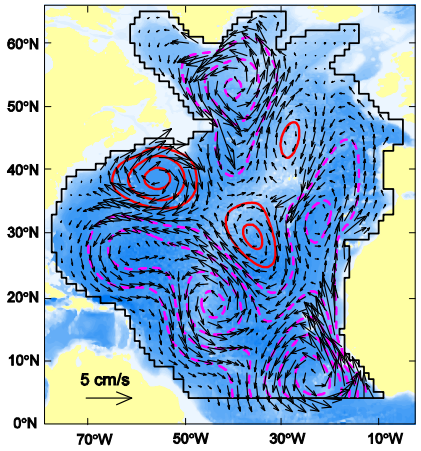

May – Jul 04

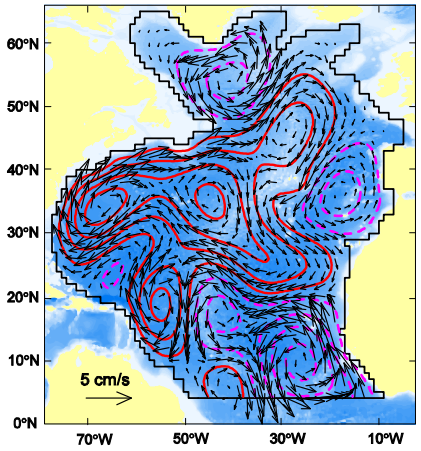

Jul-Sep 04

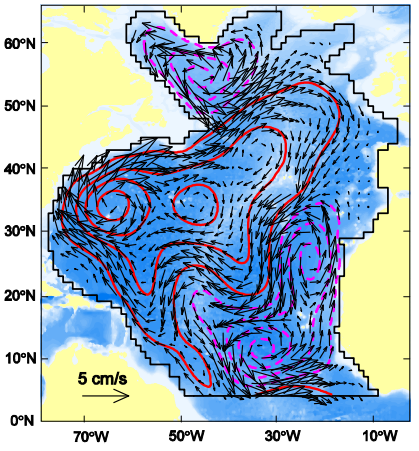

Sep – Nov 04

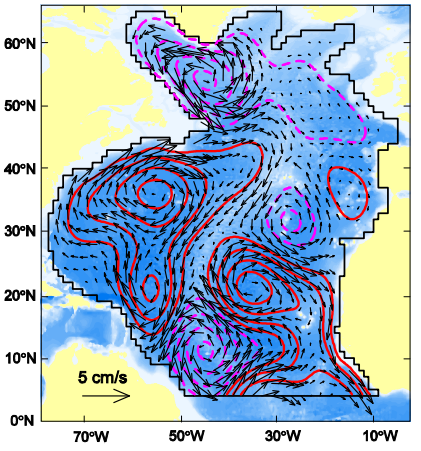

Nov 04 – Jan 05

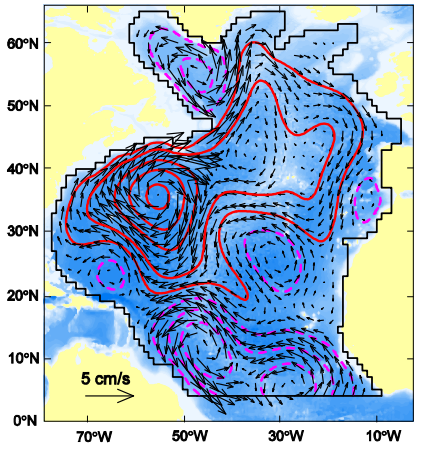

Jan-Mar 05

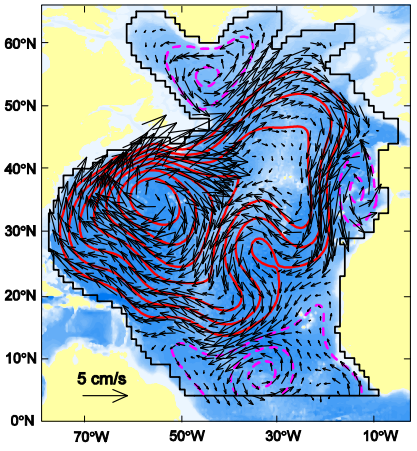

Mar – May 05

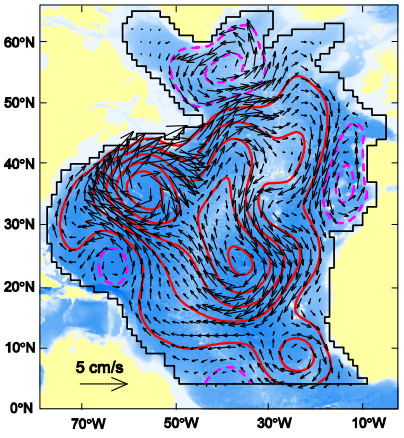

Temperature at 950 m (March 04 to May 05)

NOAA/WOA

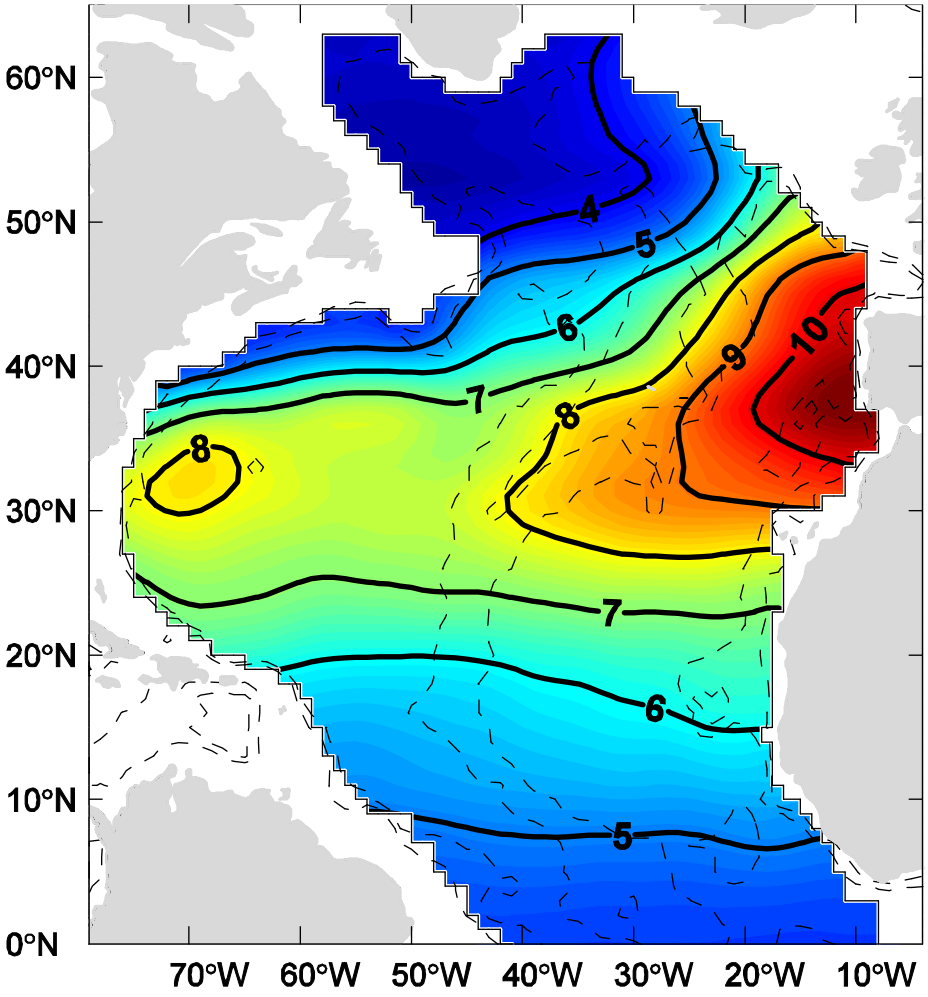

OSD

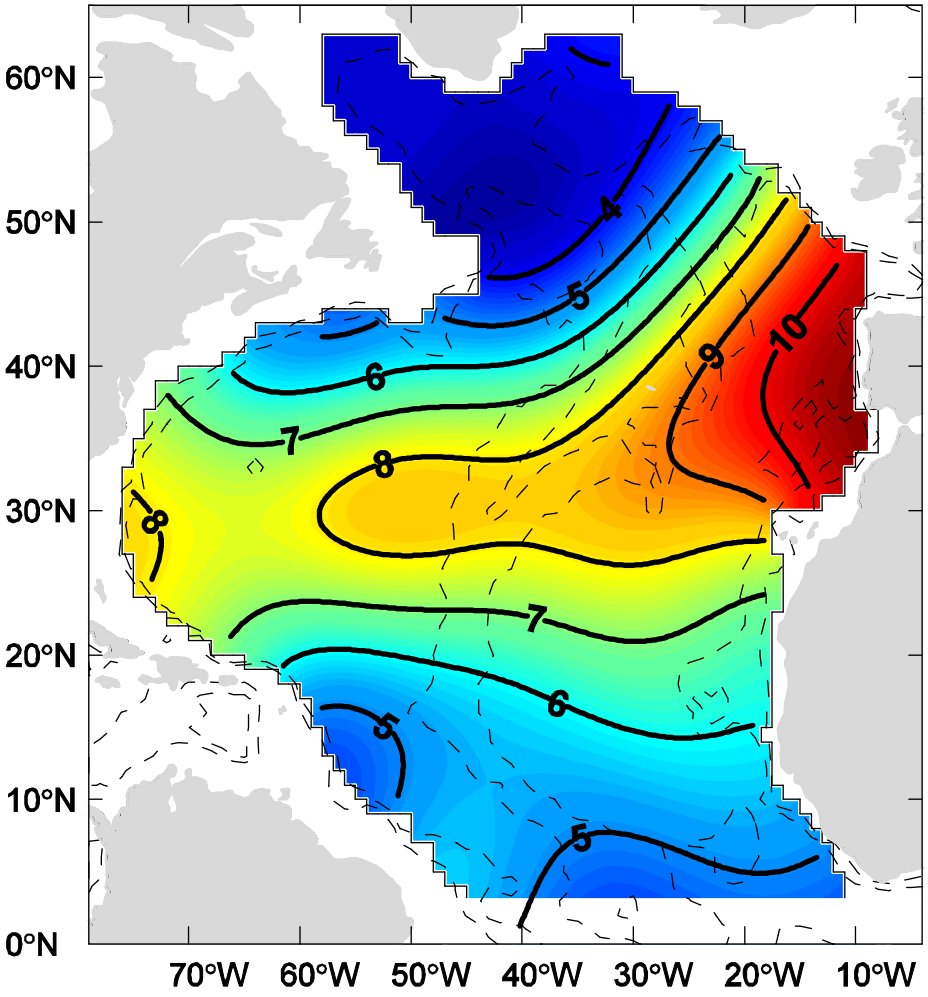

Mid-Depth Temperature (950 m)

May 04

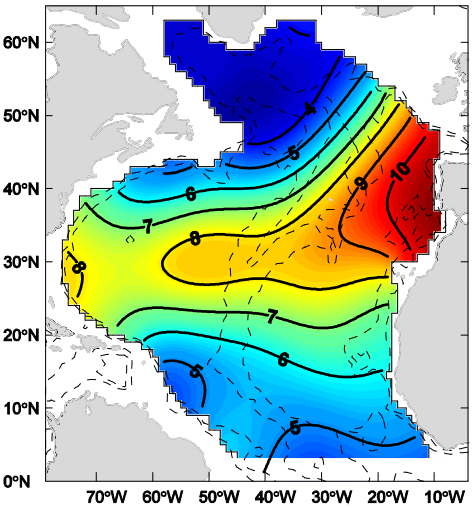

Jul 04

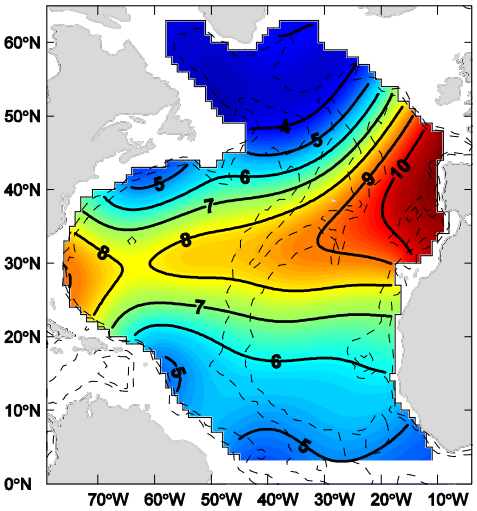

Sep 04

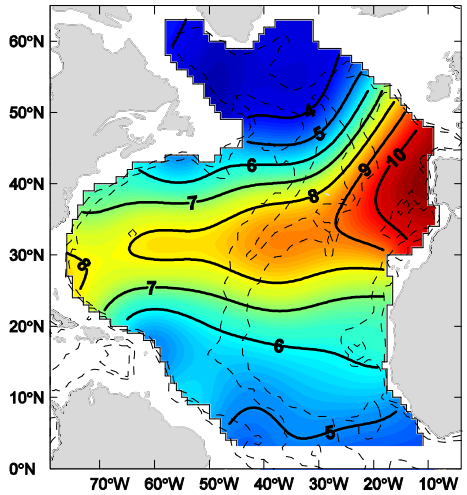

Nov 04

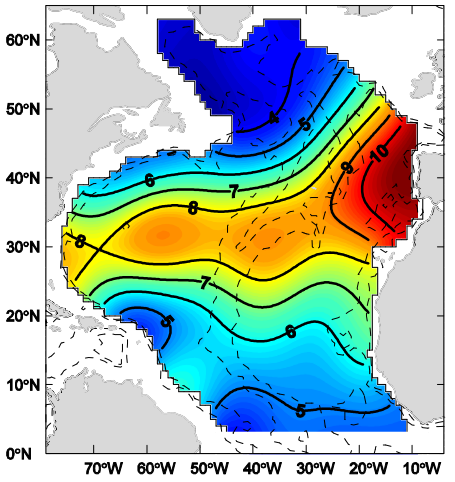

Jan 05

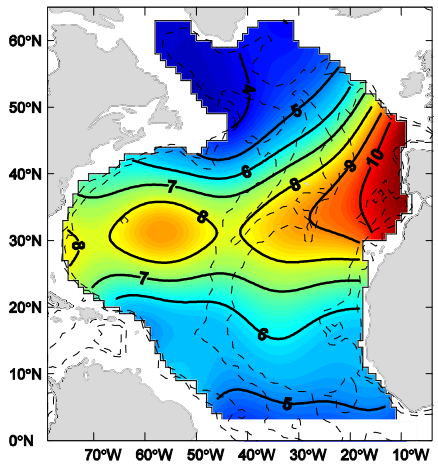

Mar 05

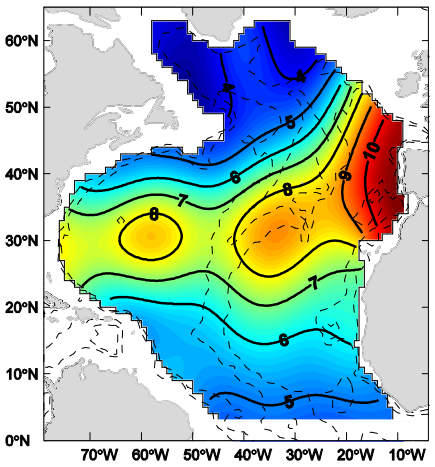

May 05

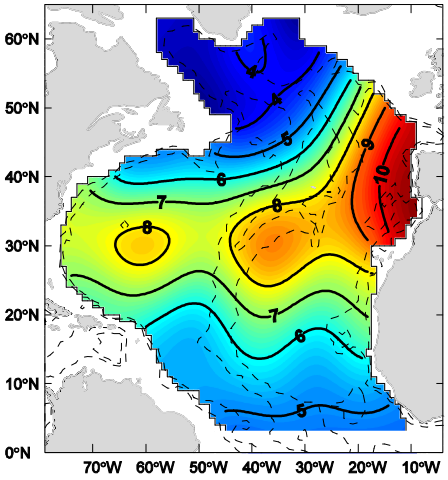

Baroclinic Rossby Waves in Tropical North Atlantic

Fourier Expansion → Temporal Annual and Semi-anuual

$$\hat{\psi} \approx \overline{\psi}(\mathbf{x}_\perp) + \psi_1(\mathbf{x}_\perp, t) + \psi_2(\mathbf{x}_\perp, t),$$

$$\psi_1(\mathbf{x}_\perp, t) = \sum_{s=1}^{2} A_{\omega_1, s} \cos(\omega_1 t + \theta_{\omega_1, s}) Z_s(\mathbf{x}_\perp) + \sum_{k=1}^{K_{opt}} B_{\omega_1, k} \cos(\omega_1 t + \vartheta_{\omega_1, k}) \Psi_k(\mathbf{x}_\perp),$$

$$\psi_2(\mathbf{x}_\perp, t) = \sum_{s=1}^{2} A_{\omega_2, s} \cos(\omega_2 t + \theta_{\omega_2, s}) Z_s(\mathbf{x}_\perp) + \sum_{k=1}^{K_{opt}} B_{\omega_2, k} \cos(\omega_2 t + \vartheta_{\omega_2, k}) \Psi_k(\mathbf{x}_\perp),$$

T_0=12 months; $\omega_1 = 2\pi / T_0$; $\omega_2 = 4\pi / T_0$

Fourier Expansion → Temporal Annual and Semi-anuual

$$\hat{T}(\mathbf{x}_\perp, z, t) \approx \overline{T}(\mathbf{x}_\perp, z) + T_1(\mathbf{x}_\perp, z, t) + T_2(\mathbf{x}_\perp, z, t),$$

$$T_1(\mathbf{x}_\perp, z, t) = \sum_{m=1}^{M_{opt}} C_{\omega_1, m}(z) \cos[\omega_1 t + \chi_{\omega_1, m}(z)] \Xi_m(\mathbf{x}_\perp, z),$$

$$T_2(\mathbf{x}_\perp, z, t) = \sum_{m=1}^{M_{opt}} C_{\omega_2, m}(z) \cos[\omega_2 t + \chi_{\omega_{21}, m}(z)] \Xi_m(\mathbf{x}_\perp, z),$$

T_0=12 months; $\omega_1 = 2\pi / T_0$; $\omega_2 = 4\pi / T_0$

Optimization

$$J_s = \int_{t_o}^{t_o+T_o} \left[a_s(t) - \sum_{\omega=\omega_1,\omega_2} A_{\omega,s} \cos(\omega t + \theta_{\omega,s}) \right]^2 dt \rightarrow \min$$

$$I_k = \int_{t_o}^{t_o+T_o} \left[b_k(t) - \sum_{\omega=\omega_1,\omega_2} B_{\omega,s} \cos(\omega t + \vartheta_{\omega,s}) \right]^2 dt \rightarrow \min$$

Annual Component

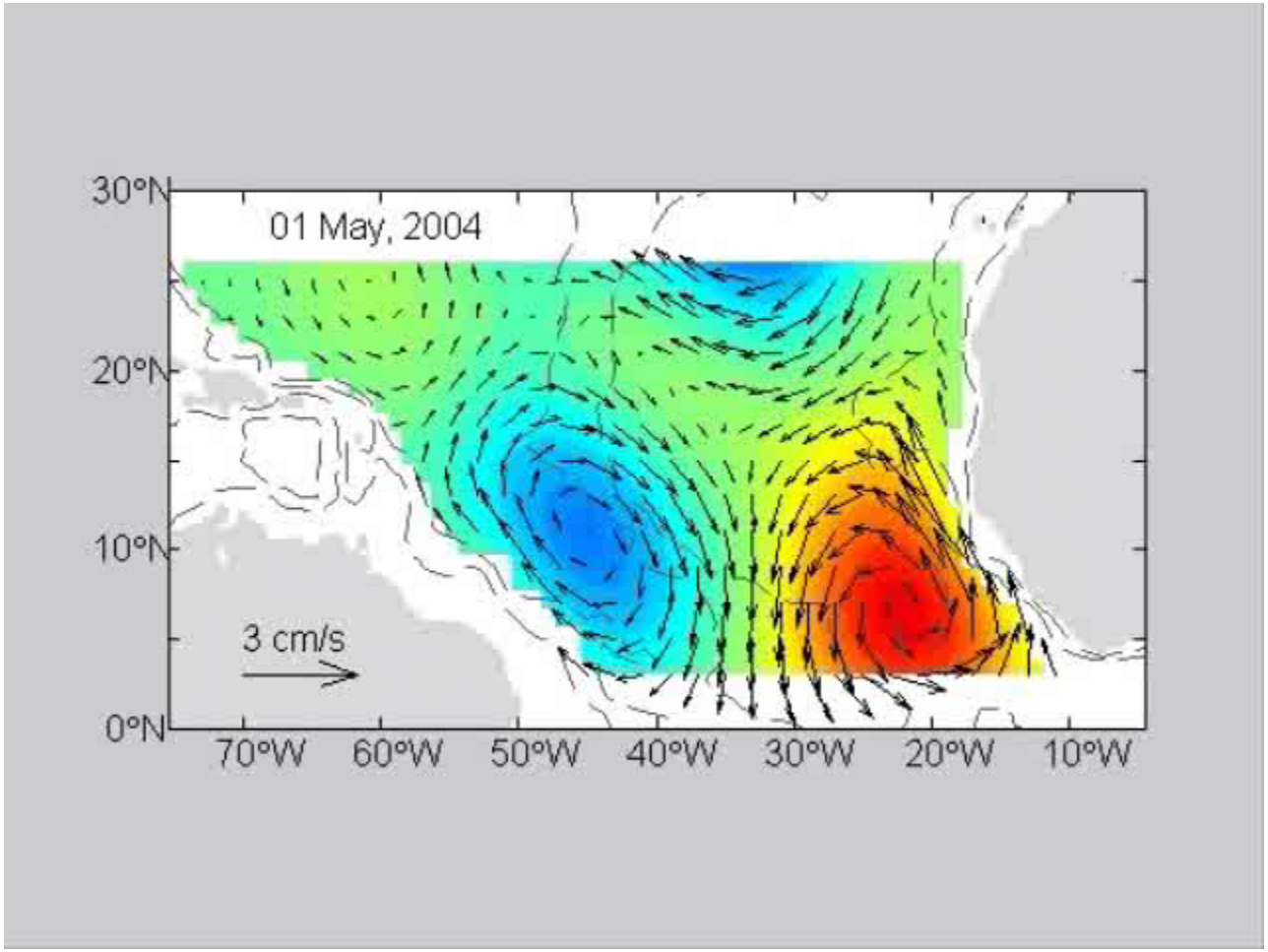

Semi-annual Component

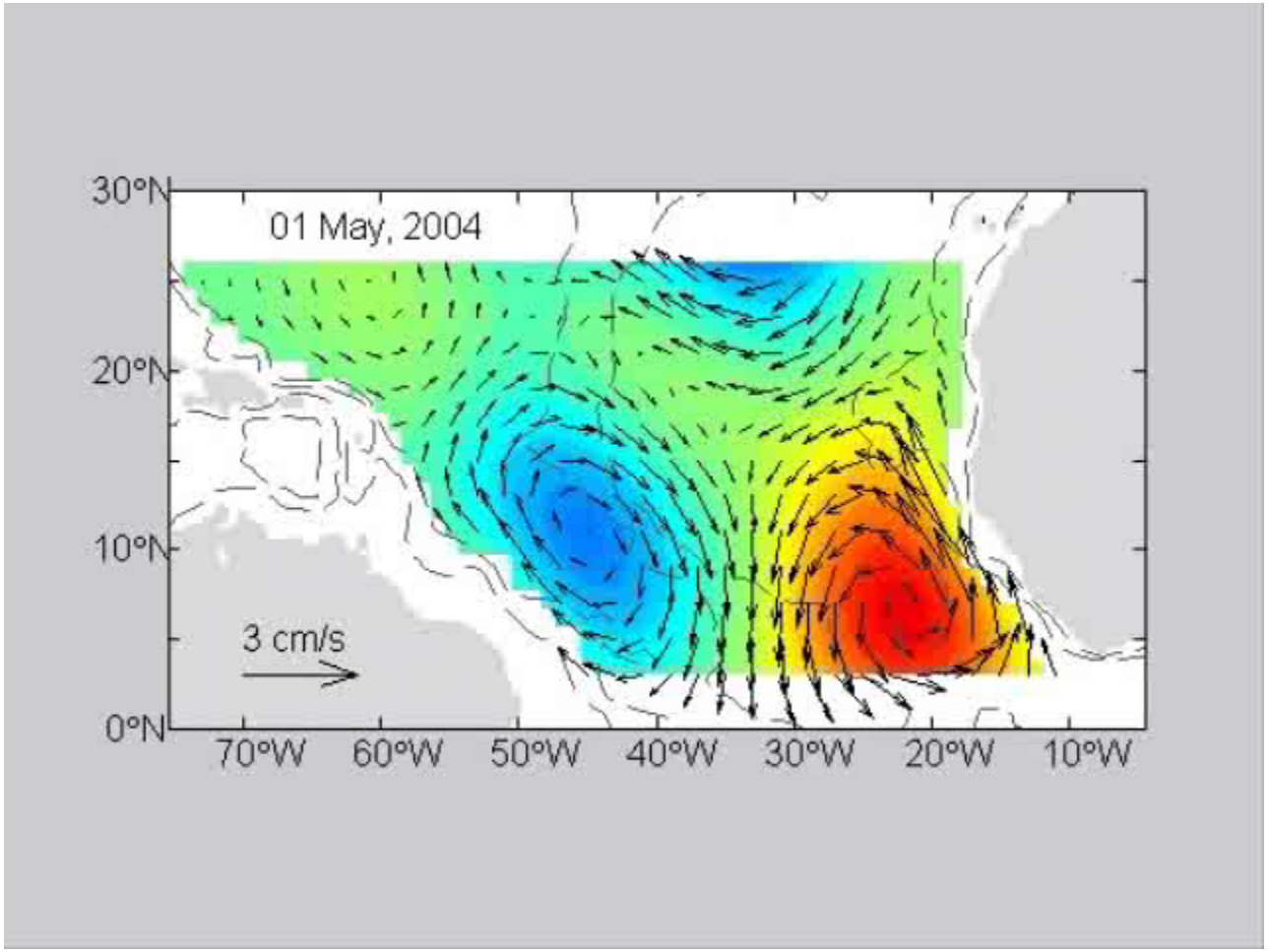

Time –Longitude Diagrams of Meridional Velocity Along 11°N

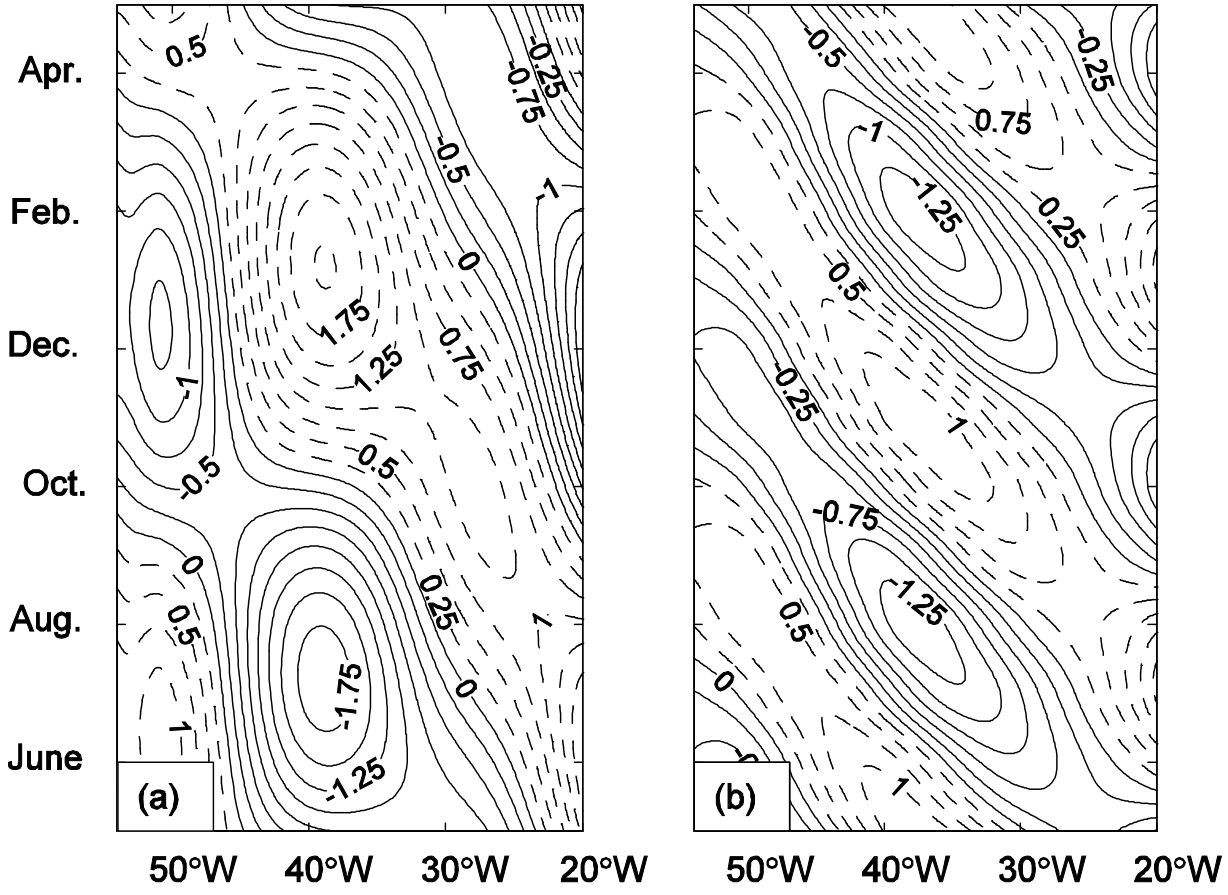

Annual

Semi-Annual

Time –Longitude Diagrams of temperature Along 11°N

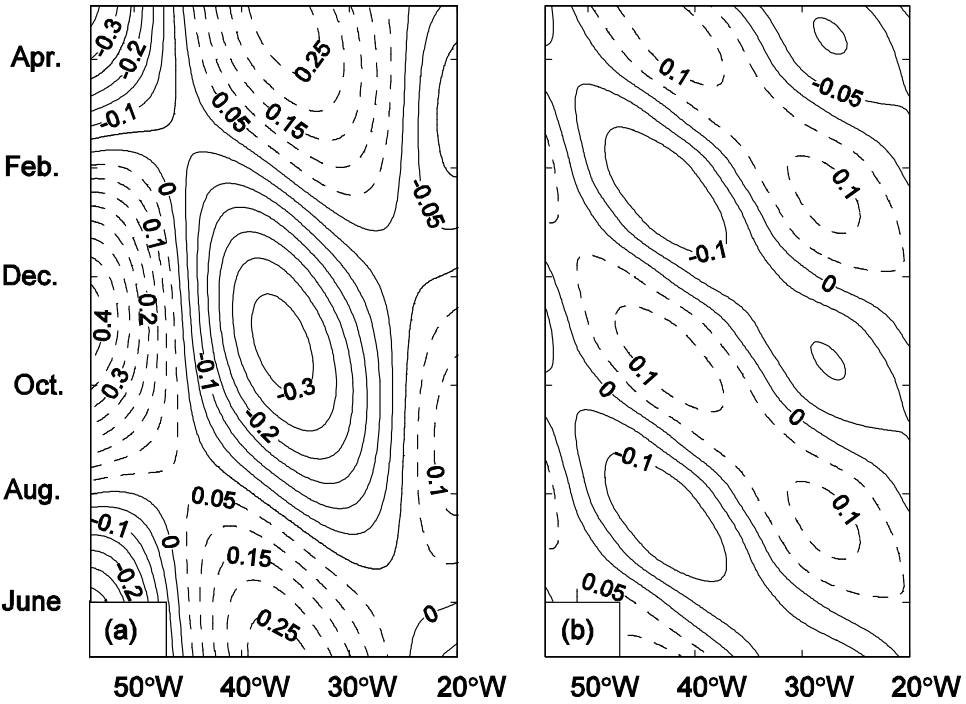

Annual

Semi-Annual

550 m

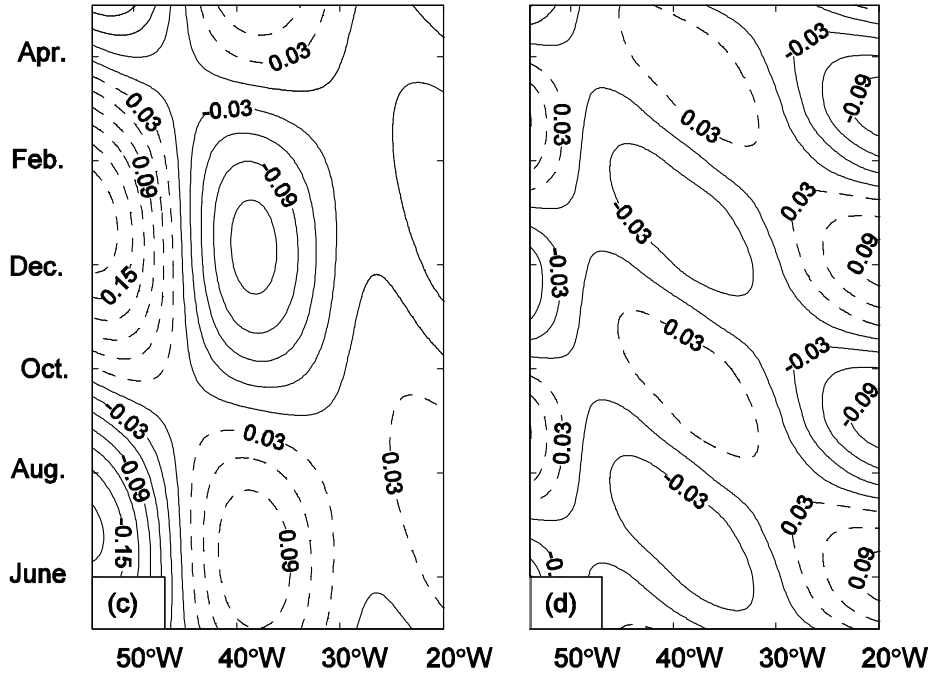

Annual

Semi-Annual

950 m

Annual Currents (1000 m)

May-Jun 2004

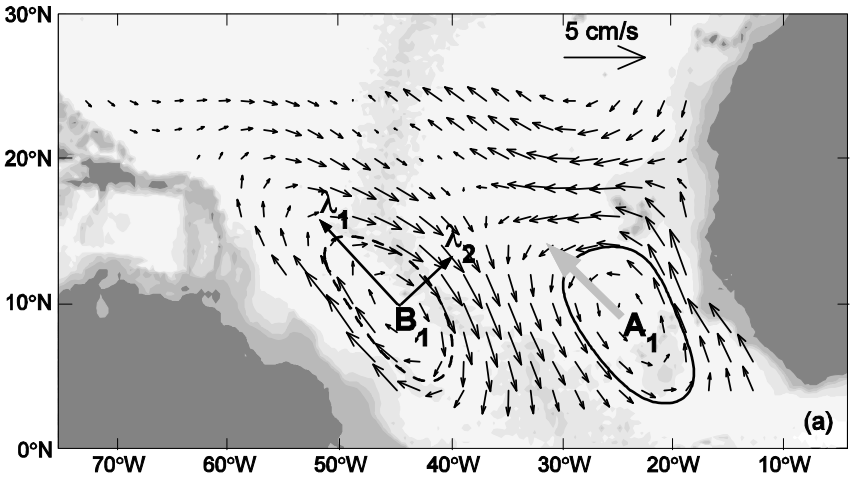

Jul-Aug 2004

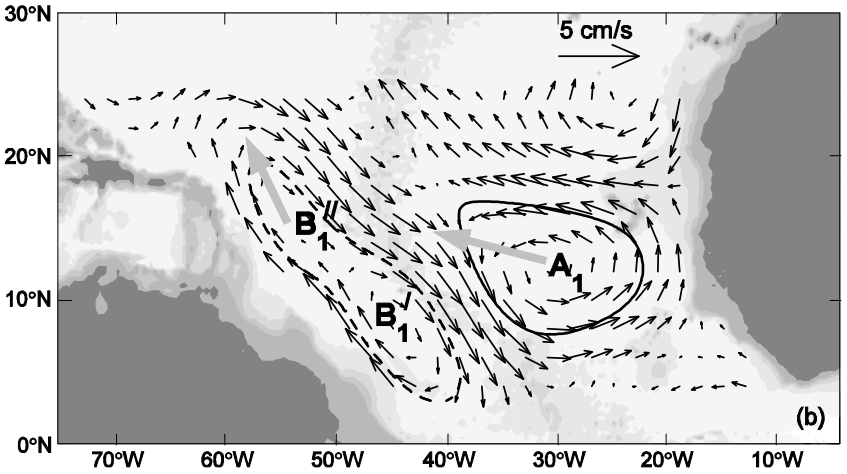

Sep-Oct 2004

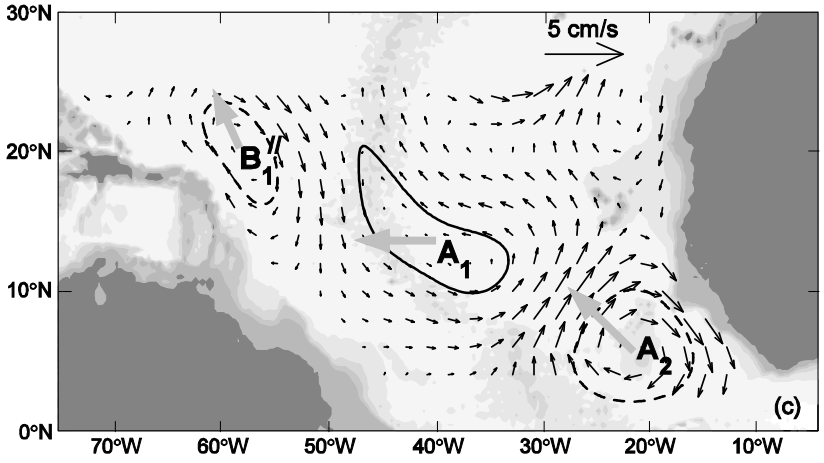

Nov-Dec 2004

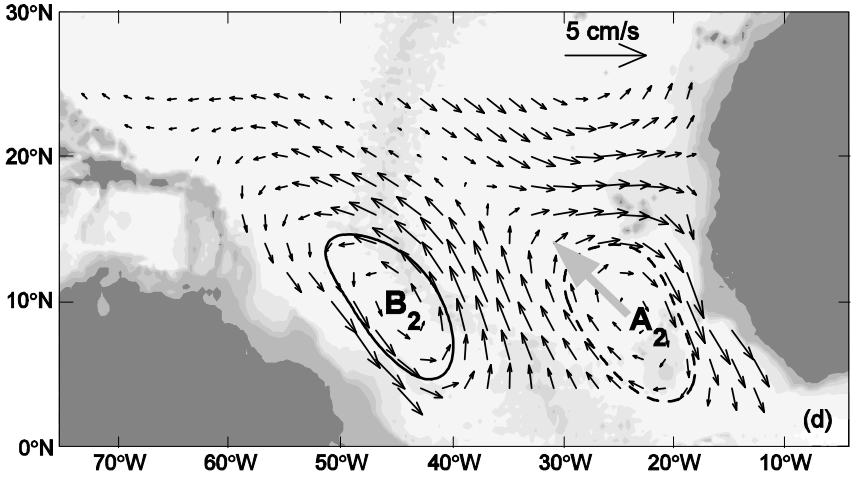

Characteristics of Annual Rossby Waves

	March, 04 – May, 05 float data			March, 04 – May, 06 float data		
Latitude	c_p (cm/s)	L_1 (km)	L_2 (km)	c_p (cm/s)	L_1 (km)	L_2 (km)
5^0N	12	1200	1100	12	1300	900
8^0N	16	2500	1400	12	2100	1100
11^0N	14	2200	1400	11	1900	1100
13^0N	11	2100	1500	10	2300	1500

Western Basin

Eastern Basin

Western Basin

Eastern Basin

Annual Monthly Temperature Anomaly (°C) at 950 m Depth - Annual Rossby Waves (7-10 cm/s)

Jun 04

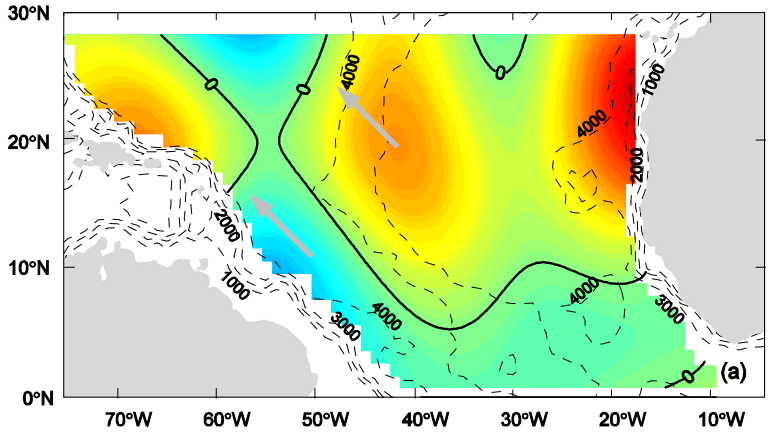

Aug 04

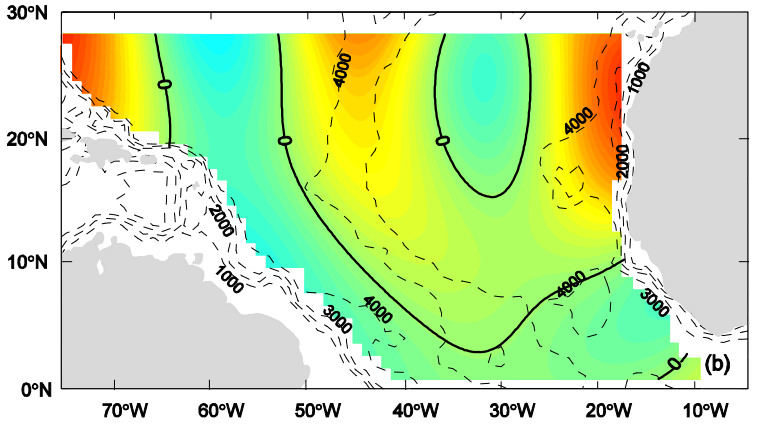

Oct 04

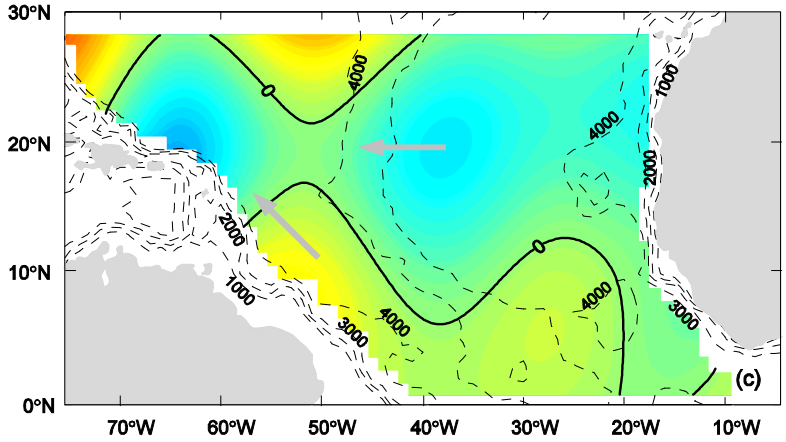

Dec 04

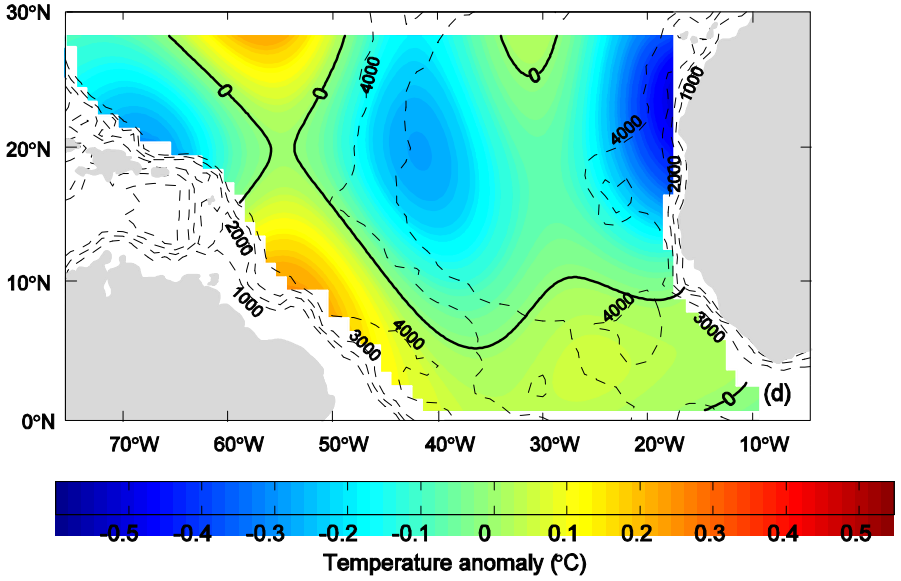

Annual Monthly Temperature Anomaly (°C) at 250 m Depth - Equatorially Forced Coastal Kelvin waves (27-30 cm/s)

Jun 04

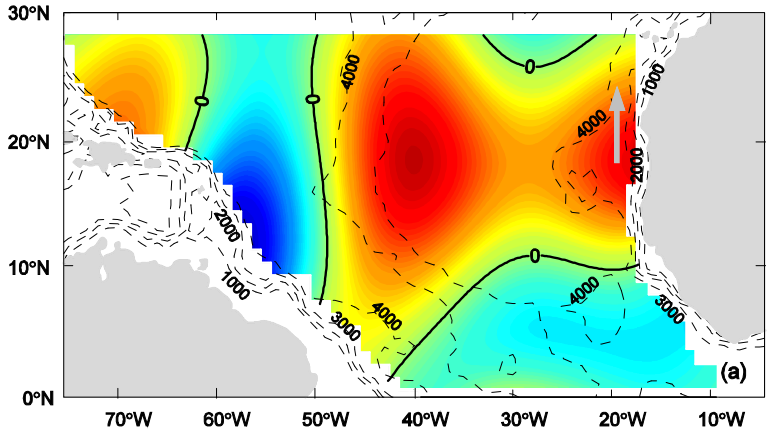

Aug 04

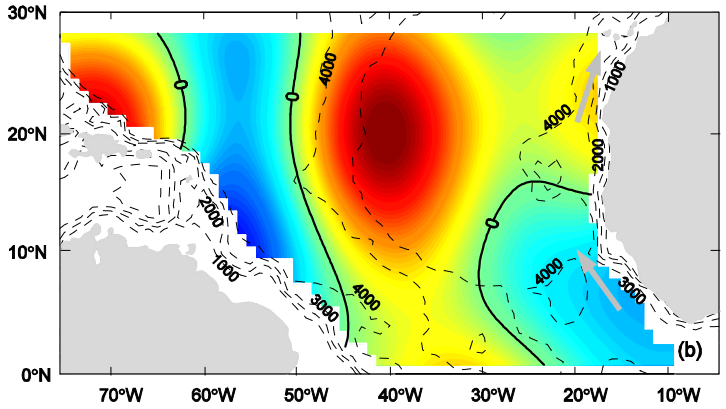

Oct 04

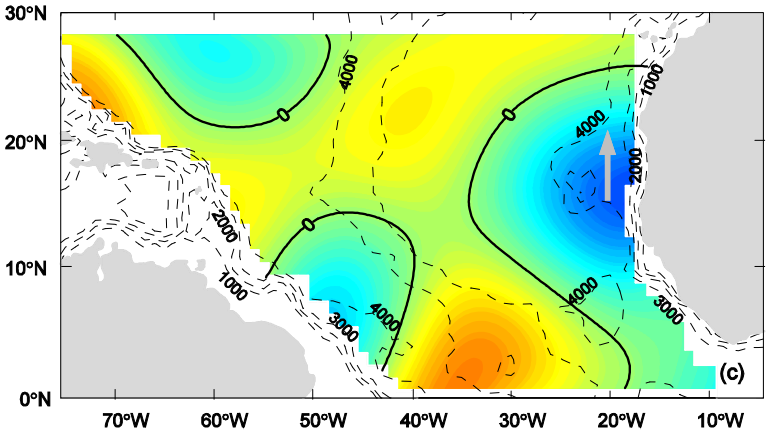

Dec 04

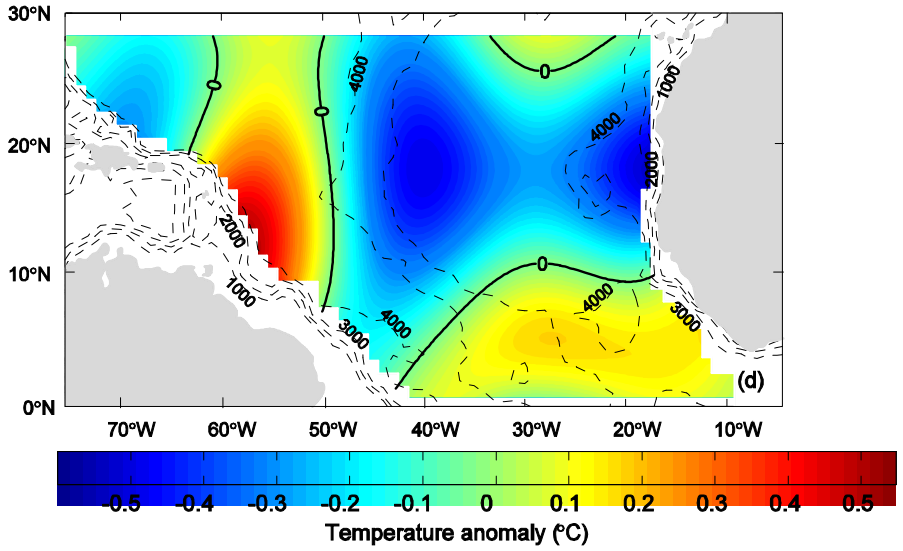

Zonal cross-sections of the annual component of the temperature anomaly (°C)

6°N in Jun 04 →

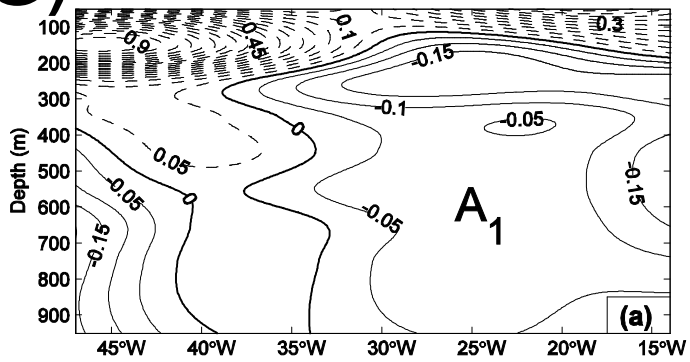

11°N in Oct, 04 →

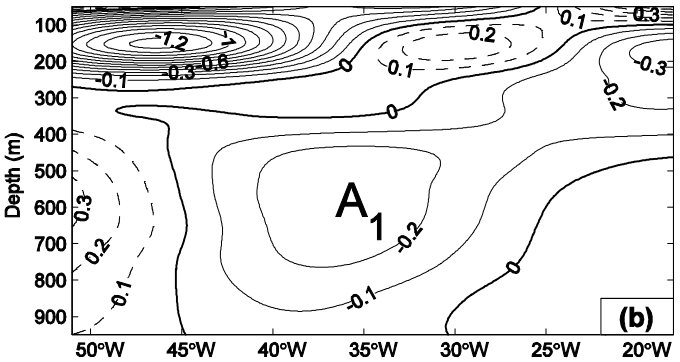

16°N in Oct 04 →

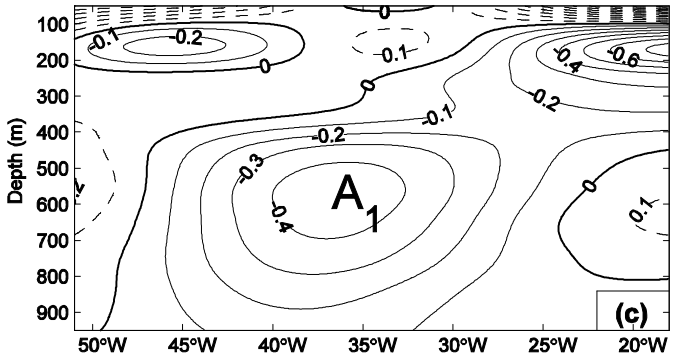

Baroclinic Modes

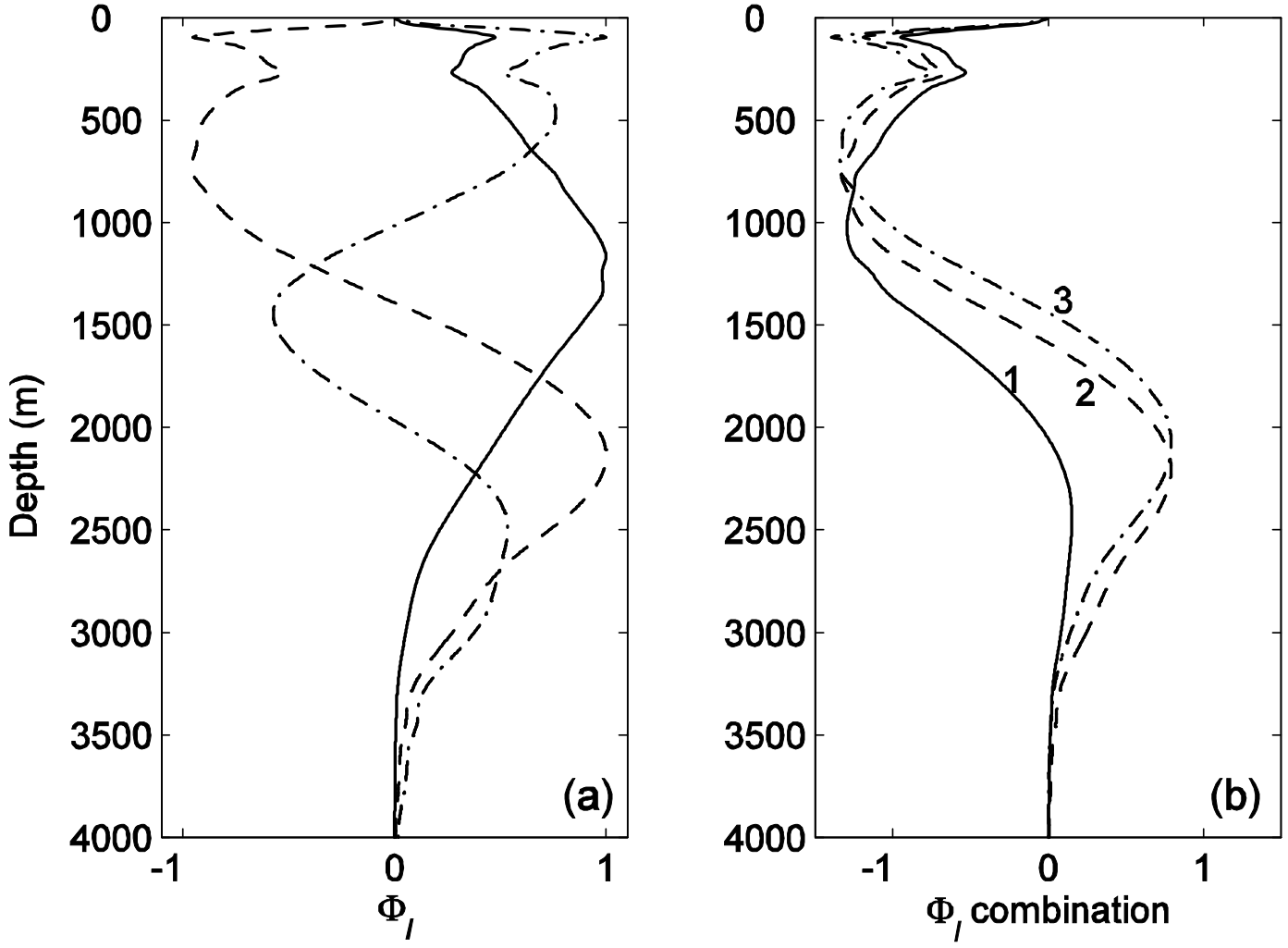

Annual Component in the Western Sub-Basin

Mean wind KE

Mean KE for mid-depth currents

Correlation between Winds and currents

Correlation between wind Stress curl and streamfunction (solid: no-lag, dashed: 3 mon lag

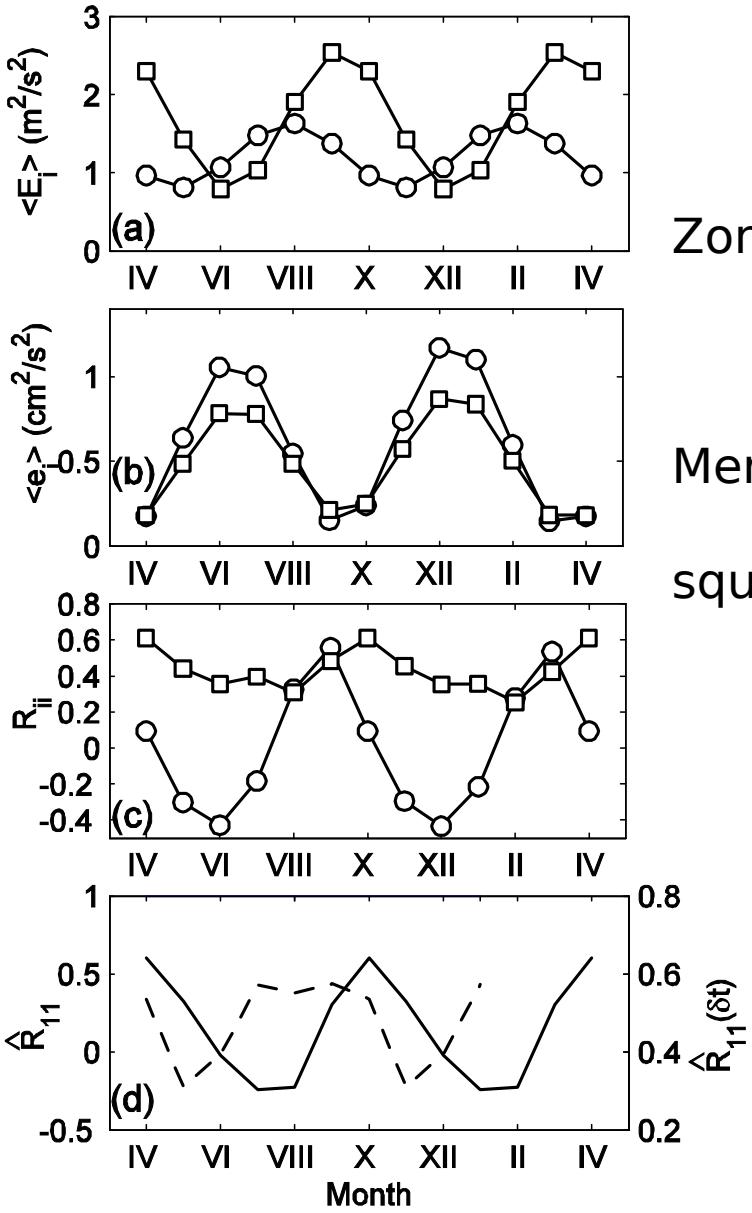

Zonal: circle

Meridional : square

Annual Component in the Eastern Sub-Basin

Mean wind KE

Mean KE for mid-depth currents

Correlation between Winds and currents

Correlation between wind Stress curl and streamfunction (solid: no-lag, dashed: 3 mon la

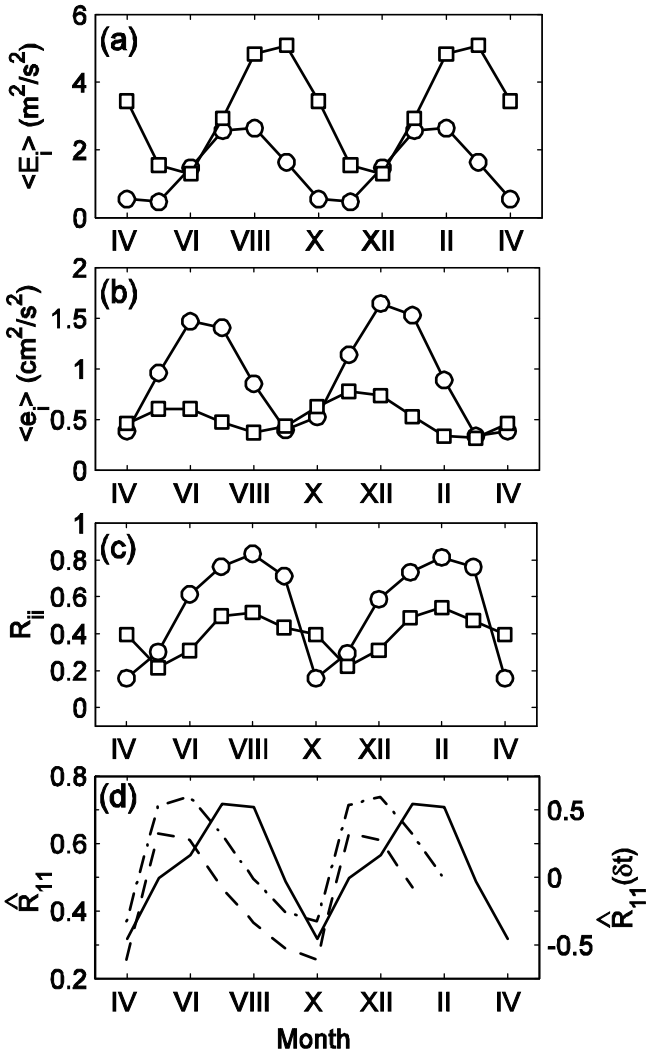

Zonal: circle

Meridional :

square

Semi-annual currents at 1000 m depth (2004)

(a)5/15
(b)5/30
(c)6/14
(d)6/29
(e) 7/13

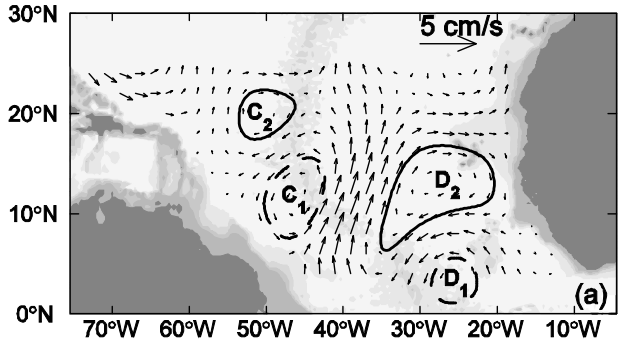

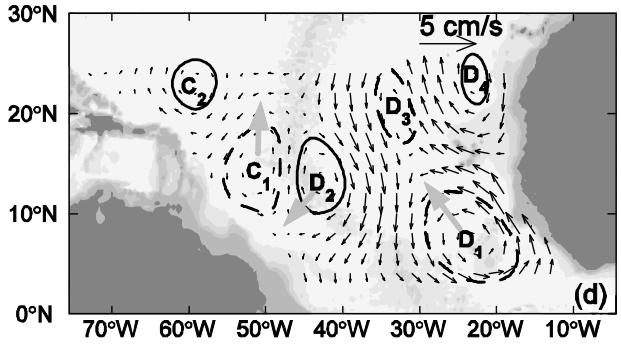

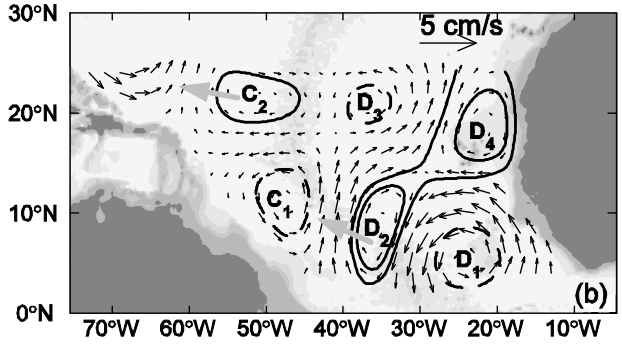

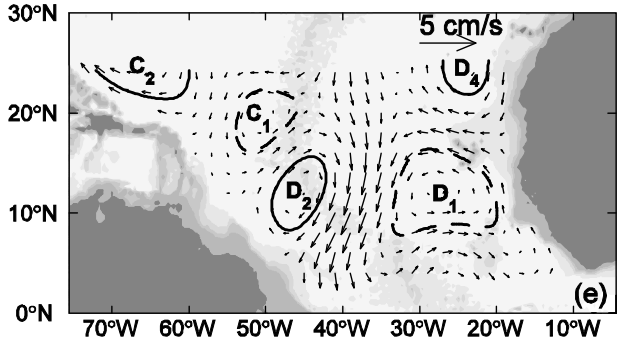

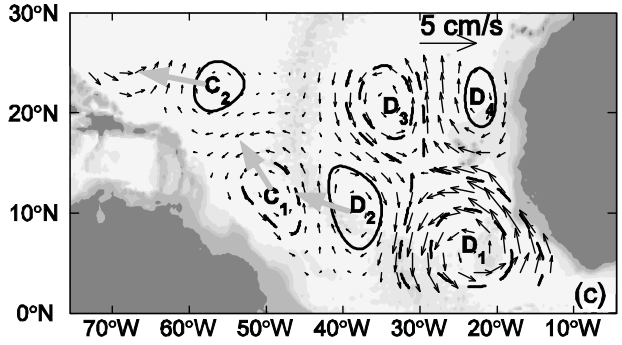

Semi-annual monthly temperature anomaly at 950m depth

a)Jun 04
b) Aug 04
c) Oct 04
d) Dec 04.

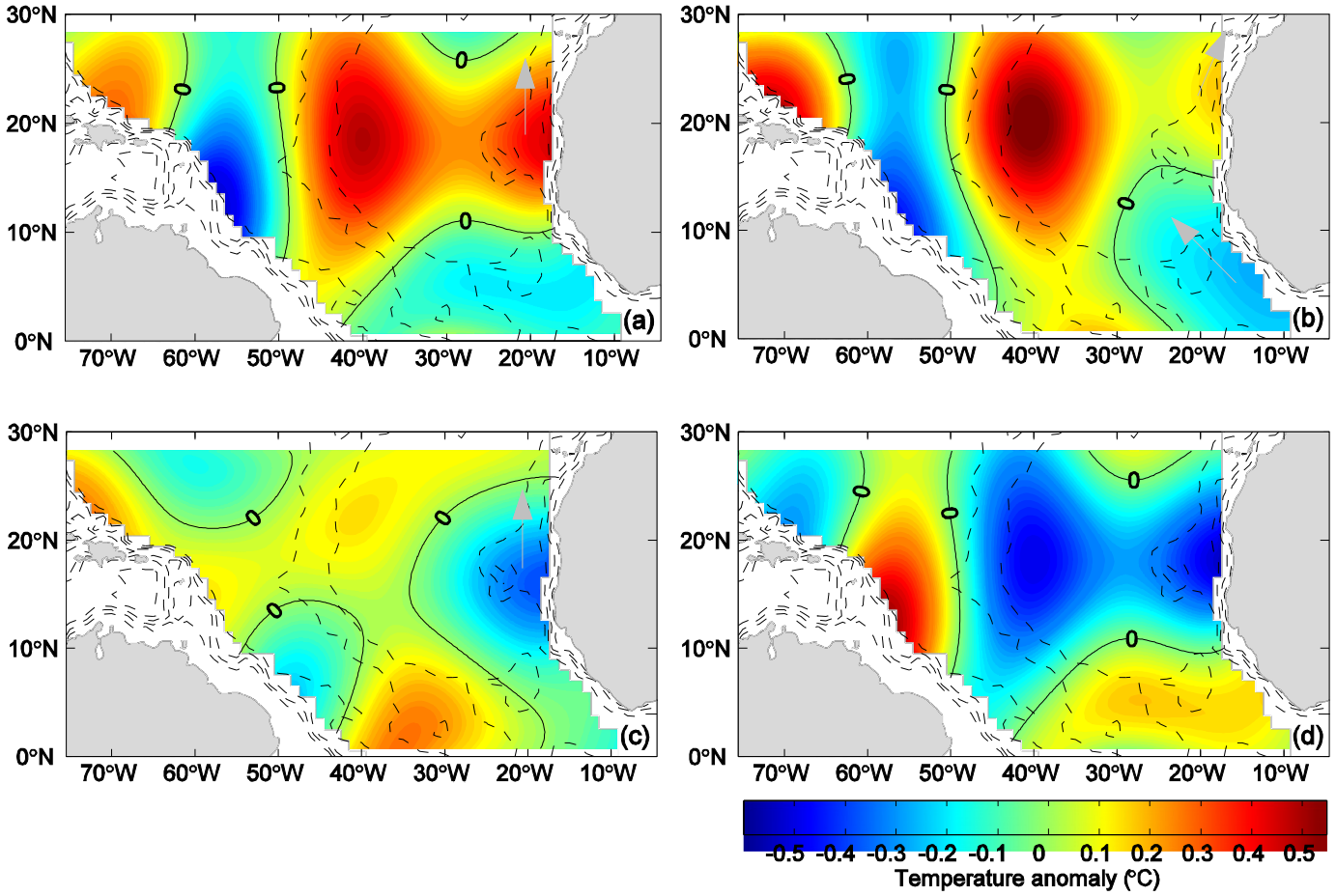

Semi-annual component of monthly temperature anomaly along 11°N (2004)

(a) 6/4
(b) 7/4
(c) 8/4
(d) 9/4

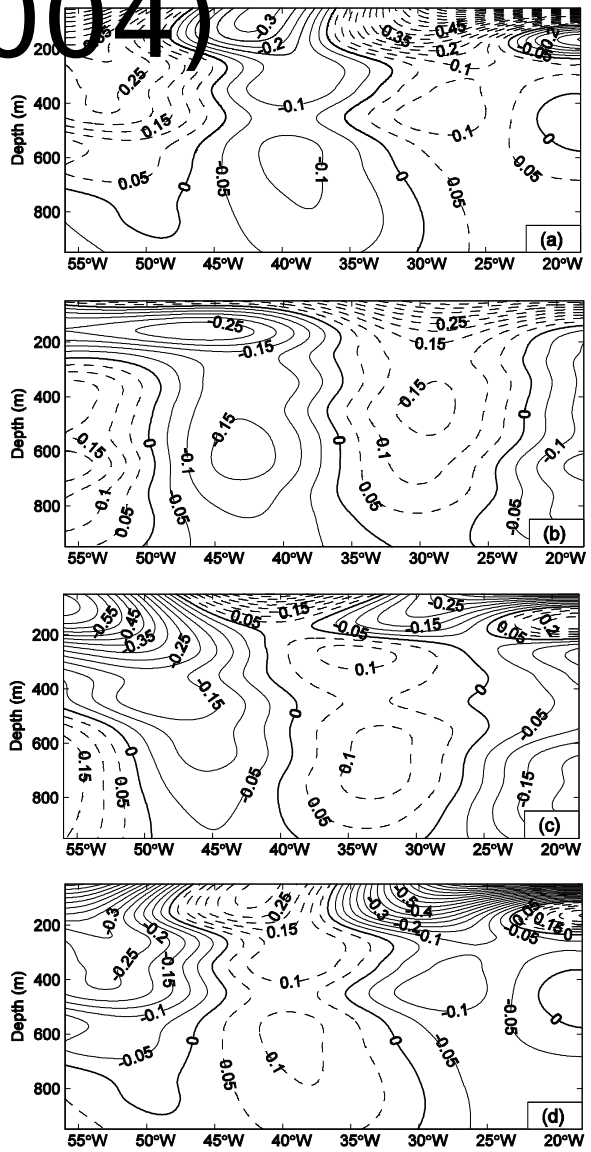

Semi-annual temperature anomaly at 550m depth (2004)

(a) 5/15

(b) 6/29

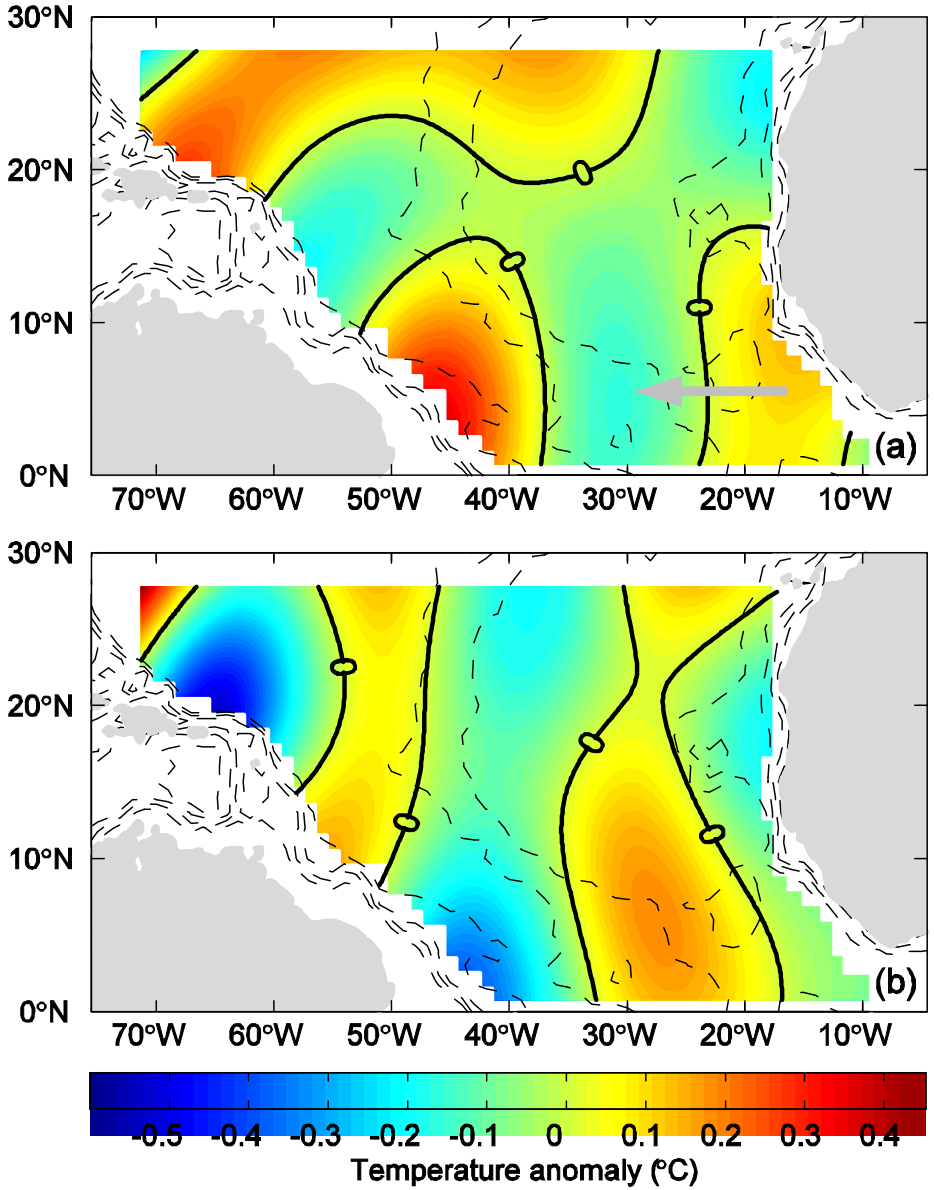

Semiannual Component in the Western Sub-Basin

(a) wind KE
(b) current KE
(c) corr wind stress and currents
(d) corr between semi-annual currents and mean wind
(e) corr between semiannual currents and annual wind stress.

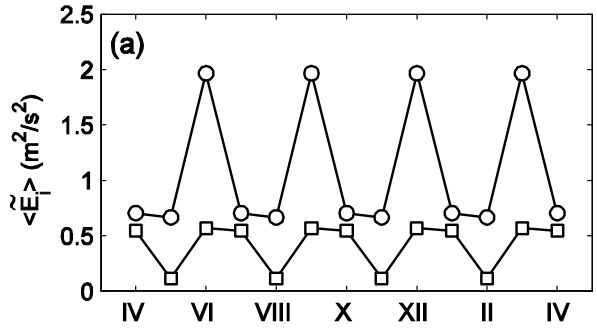

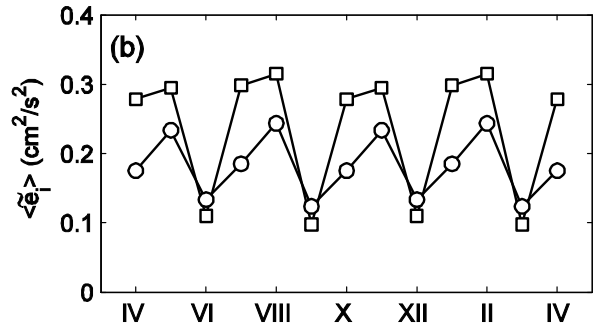

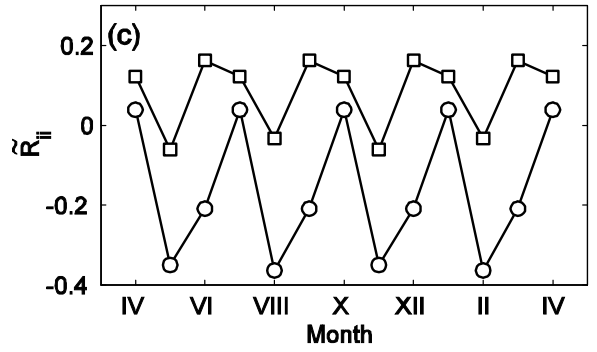

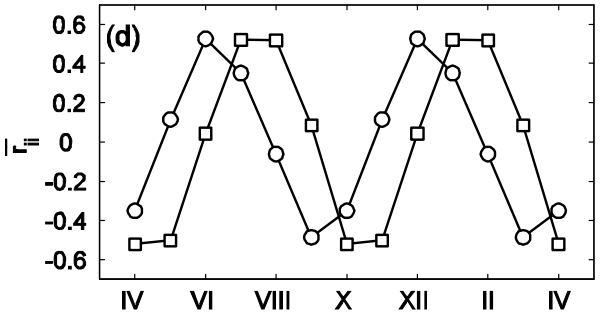

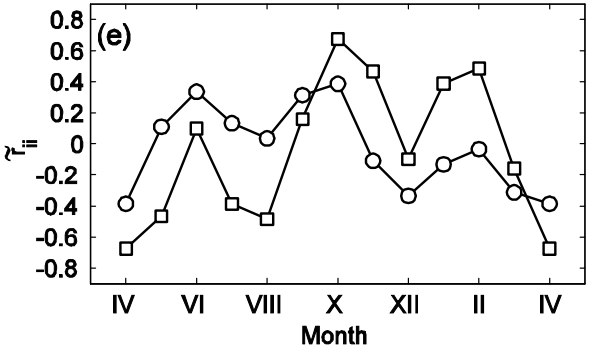

Semiannual Component in the Eastern Sub-Basin

(a) wind KE
(b) current KE
(c) corr wind stress and currents
(d) corr between semi-annual currents and mean wind
(e) corr between semiannual currents and annual wind stress.

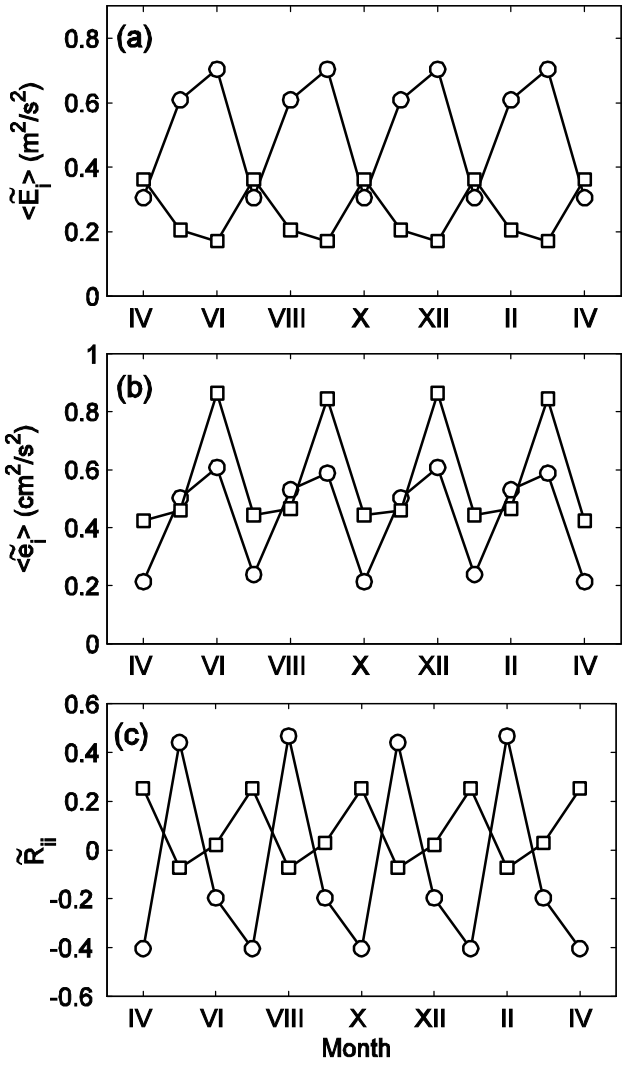

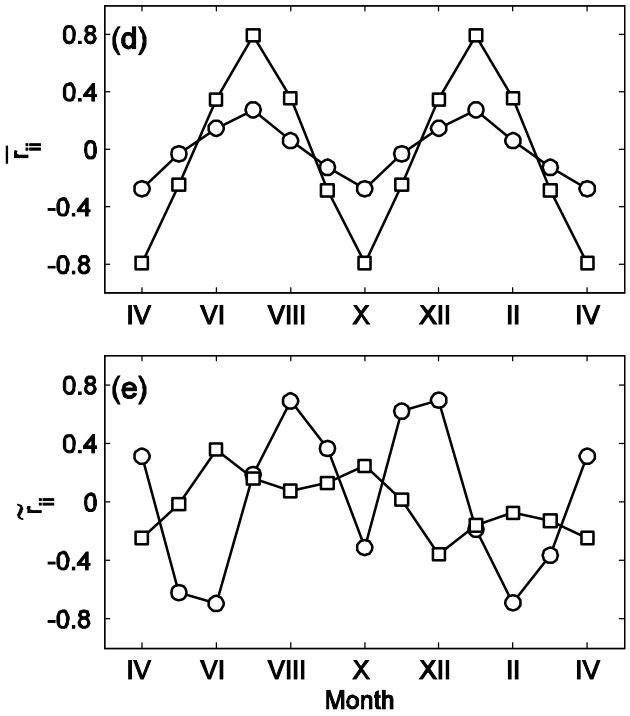

Results

- The annual and semi-annual unstable standing Rossby waves are detected in both the western and eastern sub-basins.

- The wind-driven Ekman pumping seems to be responsible for the standing wave generation in both the sub-basins.

Example-3
OSD for Analyzing Combined Current Meter and Surface Drifting Buoy Data

Ocean Velocity Observation

- 31 near-surface (10-14 m) current meter moorings during LATEX from April 1992 to November 1994

- Drifting buoys deployed at the first segment of the Surface Current and Lagrangian-drift Program (SCULP-I) from October 1993 to July 1994.

Moorings and Buoys

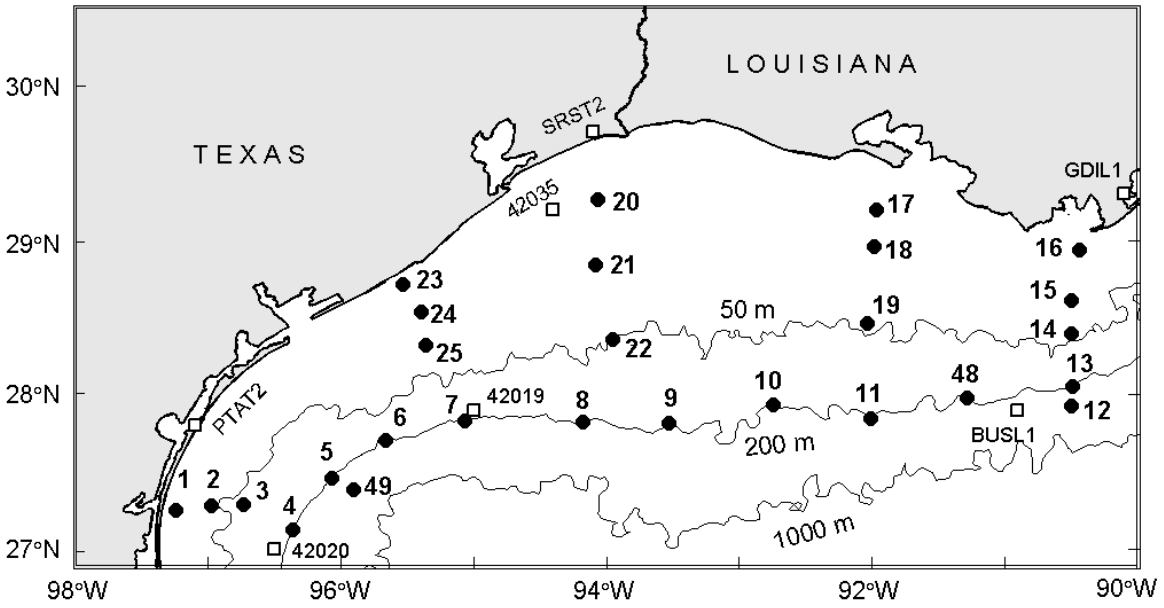

LTCS current reversal detected from SCULP-I drift trajectories.

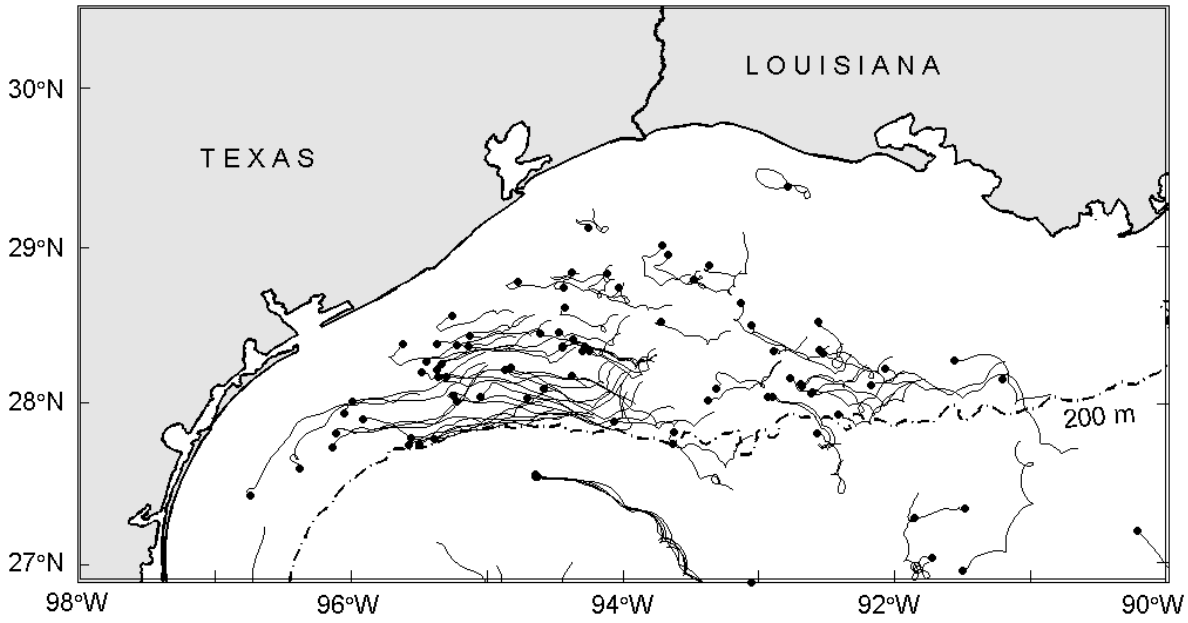

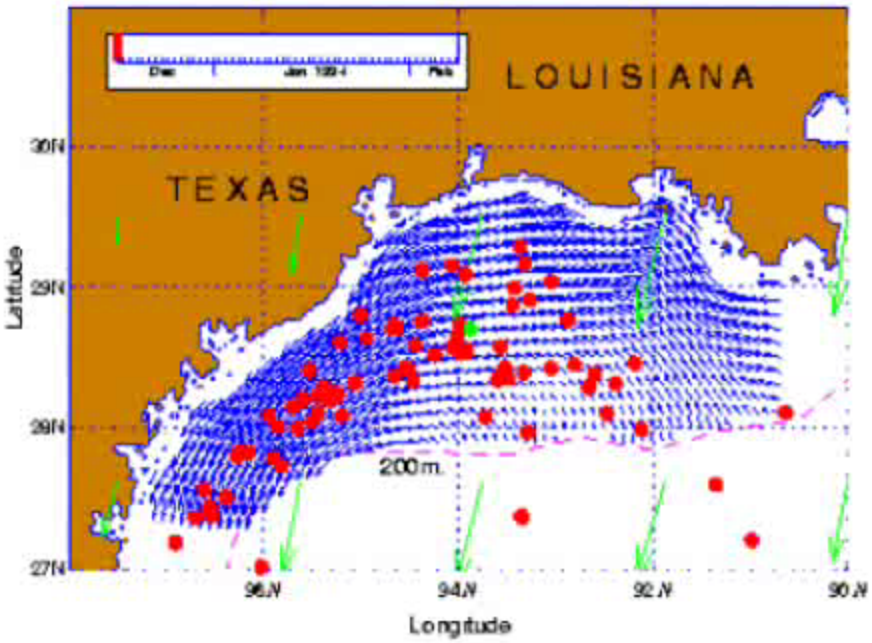
LOUISIANA
TEXAS
30N
29N
28N
27N
200m
96N
94N
92N
90N
Latitude
Longitude

Reconstructed and observed circulations at Station-24.

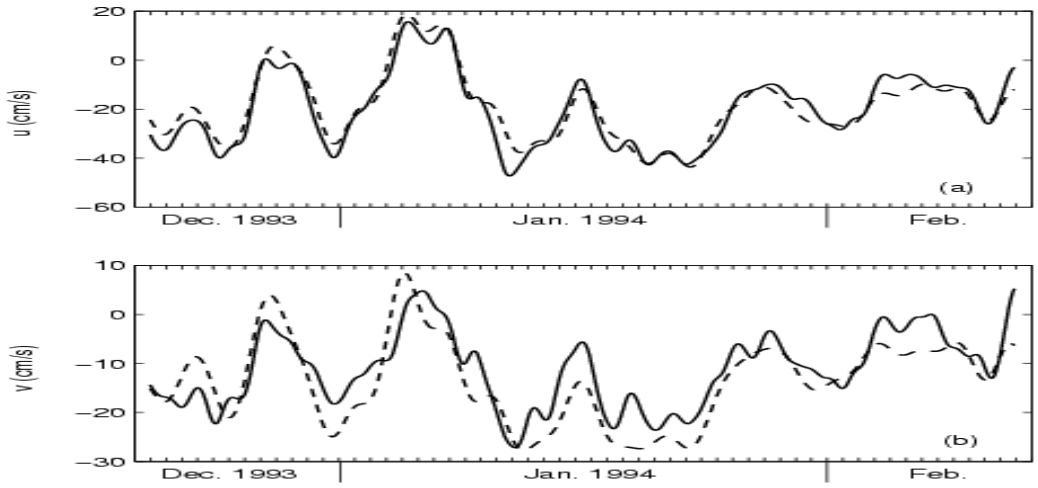

Probability of TLCS Current Reversal for Given Period (T)

- n_0 ~0-current reversal
- n_1~ 1-current reversal
- n_2~ 2-current reversals
- m ~ all realizations

$$P_0(T) = \frac{n_0}{m}, P_1(T) = \frac{n_1}{m}, P_2(T) = \frac{n_2}{m},$$

Fitting the Poison Distribution

$$P_k(T) = \frac{1}{k!}(\mu T)^k \exp(-\mu T)$$

k=0, 1, 2

μ is the mean number of reversal for a single time interv

μ ~ 0.08

Dependence of P_0, P_1, P_2 on T

For observational periods larger than 20 days, the probability for no current reversal is less than 0.2.

For 15 day observational period, the probability for 1-reversal reaches 0.5

Data – Solid Curve
Poison Distribution Fitting – Dashed Curve

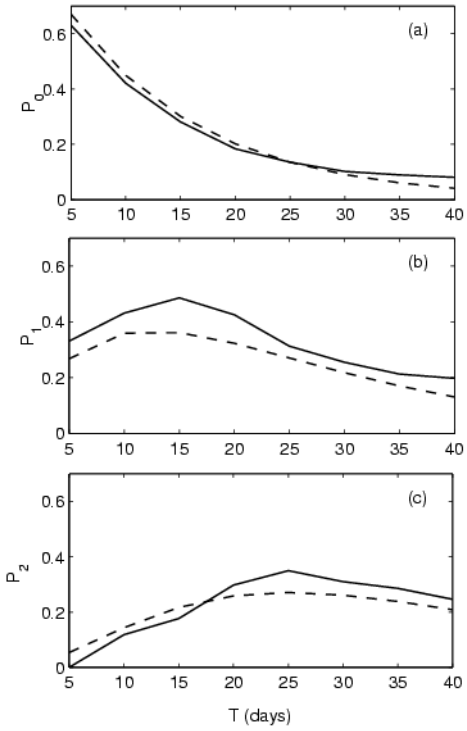

Time Interval between Successive Current Reversals (not a Rare Event)

$$p(\tau) = \mu \exp(-\mu\tau)$$

LTCS current reversal detected from the reconstructed velocity data

December 30, 1993

January 3, 1994

January 6, 1994

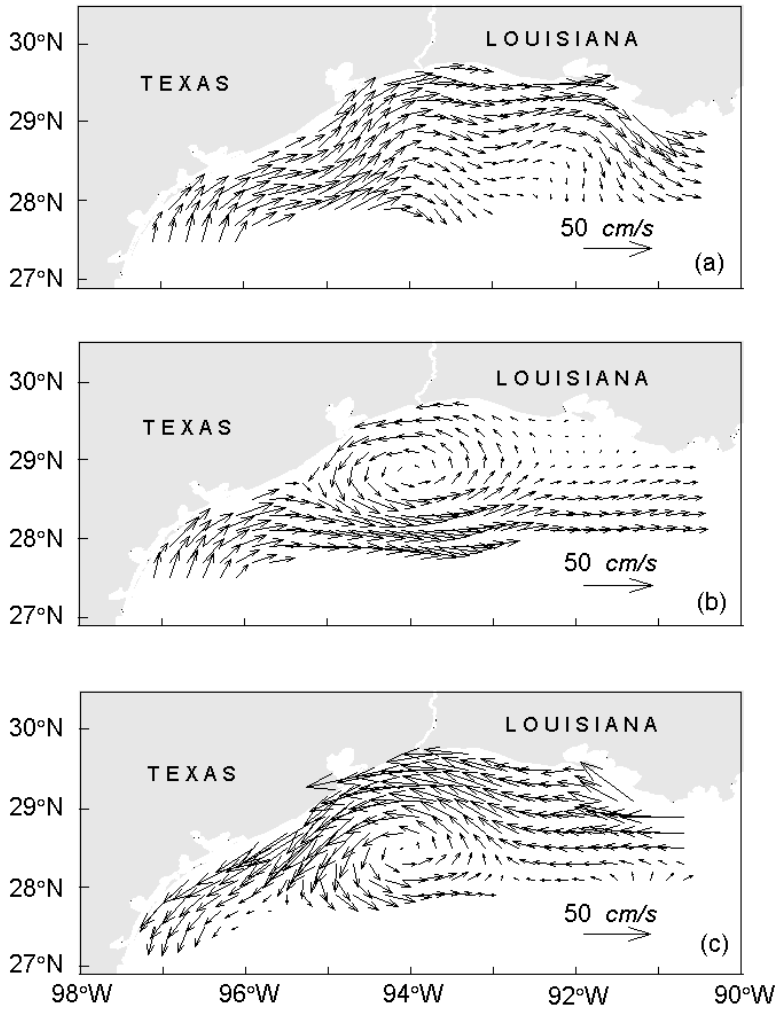

EOF Analysis of the Reconstructed Velocity Filed

EOF	Variance (%)		
	01/21/93-05/21/93	12/19/93-04/17/94	10/05/94-11/29/94
1	80.2	77.1	74.4
2	10.1	9.5	9.3
3	3.9	5.6	6.9
4	1.4	3.3	4.6
5	1.1	1.4	2.3
6	0.7	1.1	0.8

Mean and First EOF Mode

$$\tilde{\mathbf{u}}(x, y, t) = \overline{\mathbf{u}}(x, y) + A_1(t)\mathbf{u}_1(x, y),$$

Mean Circulation

1. First Period (01/21-05/21/93)

2. Second Period 12/19/93-04/17/94)

3. Third Period (10/05-11/29/94)

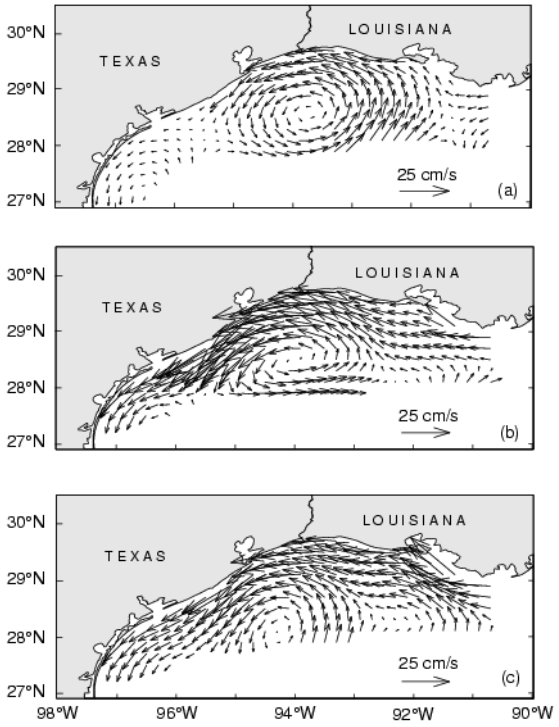

EOF1

1. First Period (01/21-05/21/93)

2. Second Period 12/19/93-04/17/94)

3. Third Period (10/05-11/29/94)

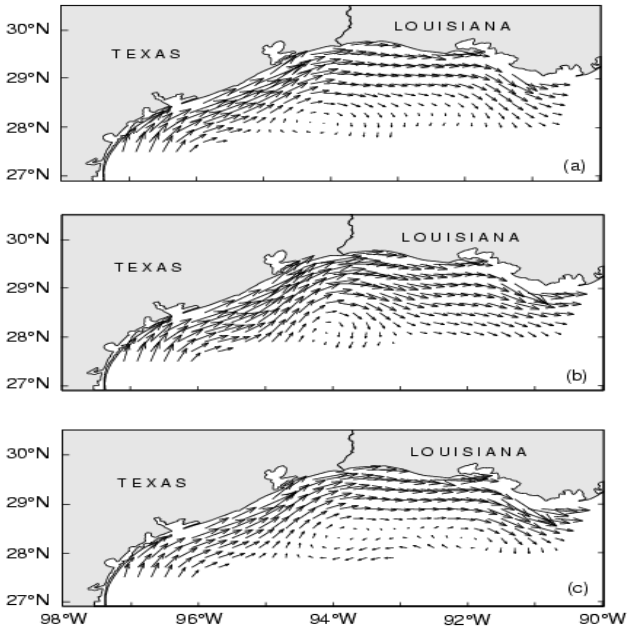

- Calculated $A_1(t)$

Using Current Mete

Mooring (solid)

and SCULP-1

Drifters (dashed)

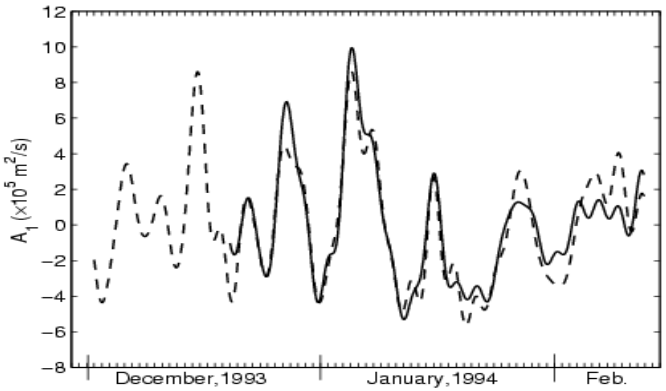

- 8 total reversals observed

$$\eta = A_1^2 / \sum_{n=2}^{6} A_n^2$$

- U_{als} ~ alongshore wind

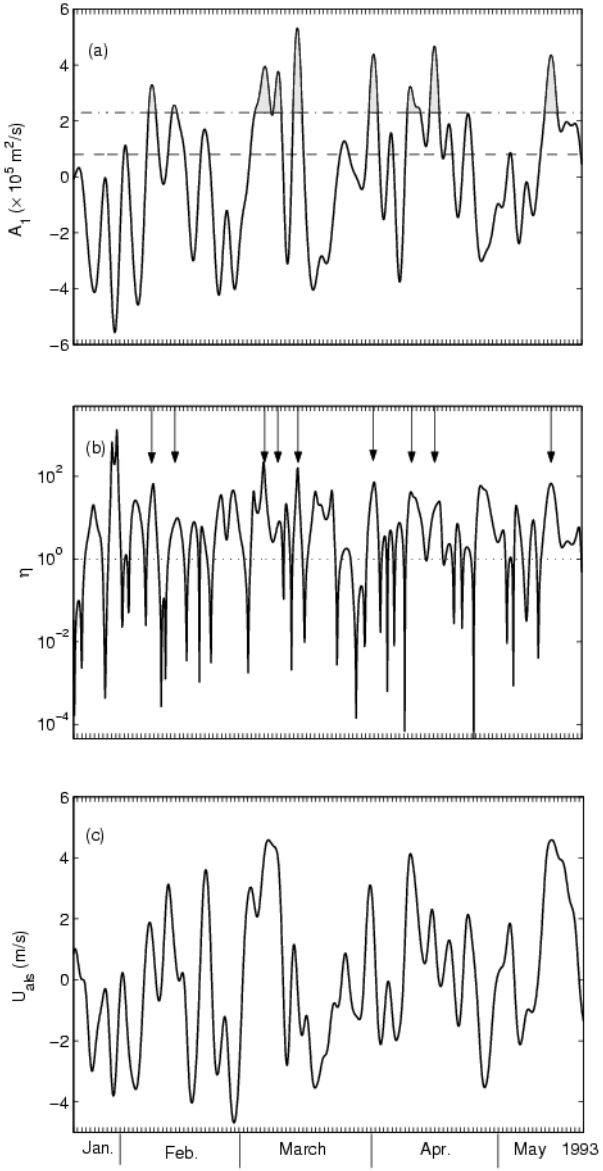

Morlet Wave

- $A_1(t)$
- U_{als}

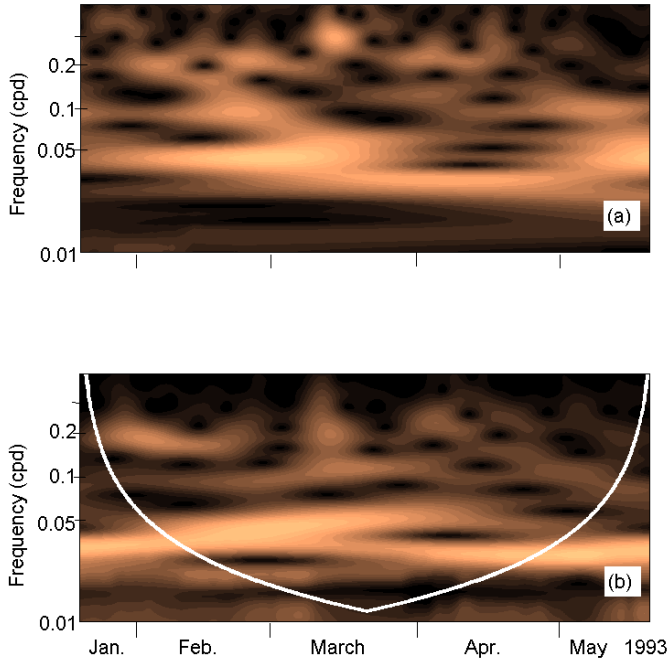

$$\Phi(t) = \pi^{-4} \exp(imt - t^2/2), \quad \mathrm{m} = 6$$

Surface Wind Data

- **7 buoys of the National Data Buoy Center (NDBC) and industry (C-MAN) around LATEX area**

- Regression between
- $A_1(t)$ and Surface
- Winds

- Solid Curve (reconstructed)
- Dashed Curve (predicted using winds)

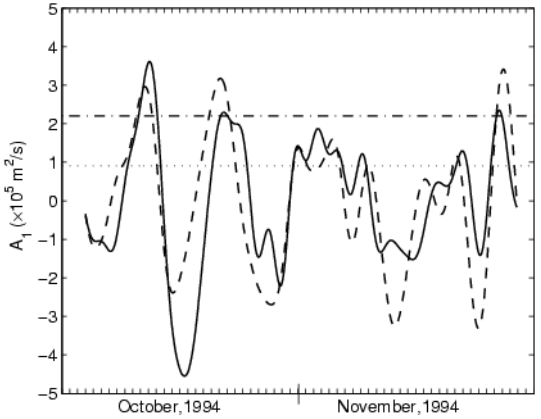

$$A_1(t) = \alpha\left[U(t) - \overline{U}\right] + \beta\left[V(t) - \overline{V}\right] + \gamma$$

Results

- Alongshore wind forcing is the major factor causing the synoptic current reversal.

- Other factors, such as the Mississippi-Atchafalaya River discharge and offshore eddies of Loop Current origin, may affect the reversal threshold, but can not cause the synoptic current reversal.

Part-4
OSD for Analyzing CODAR Data

CODAR

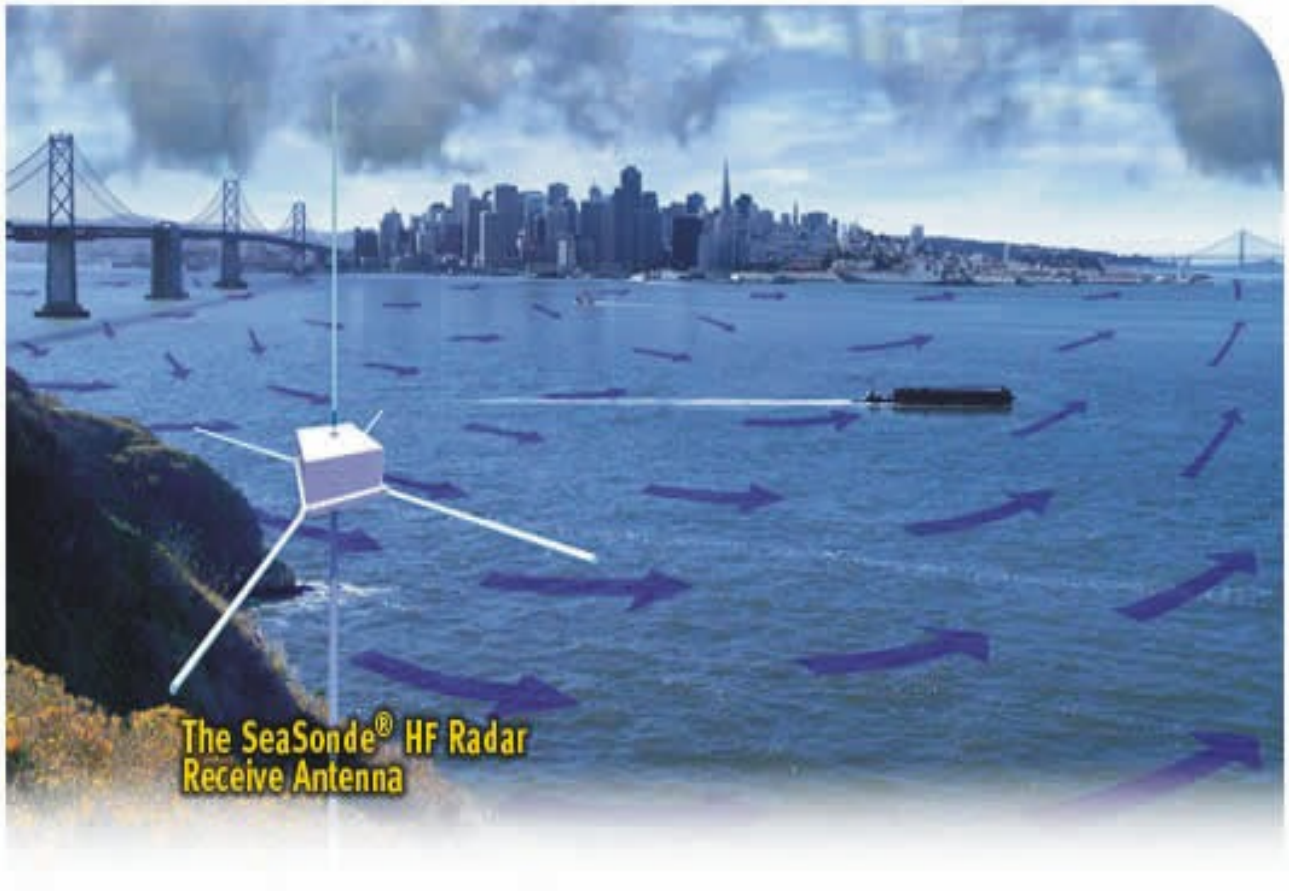

Monterey Bay

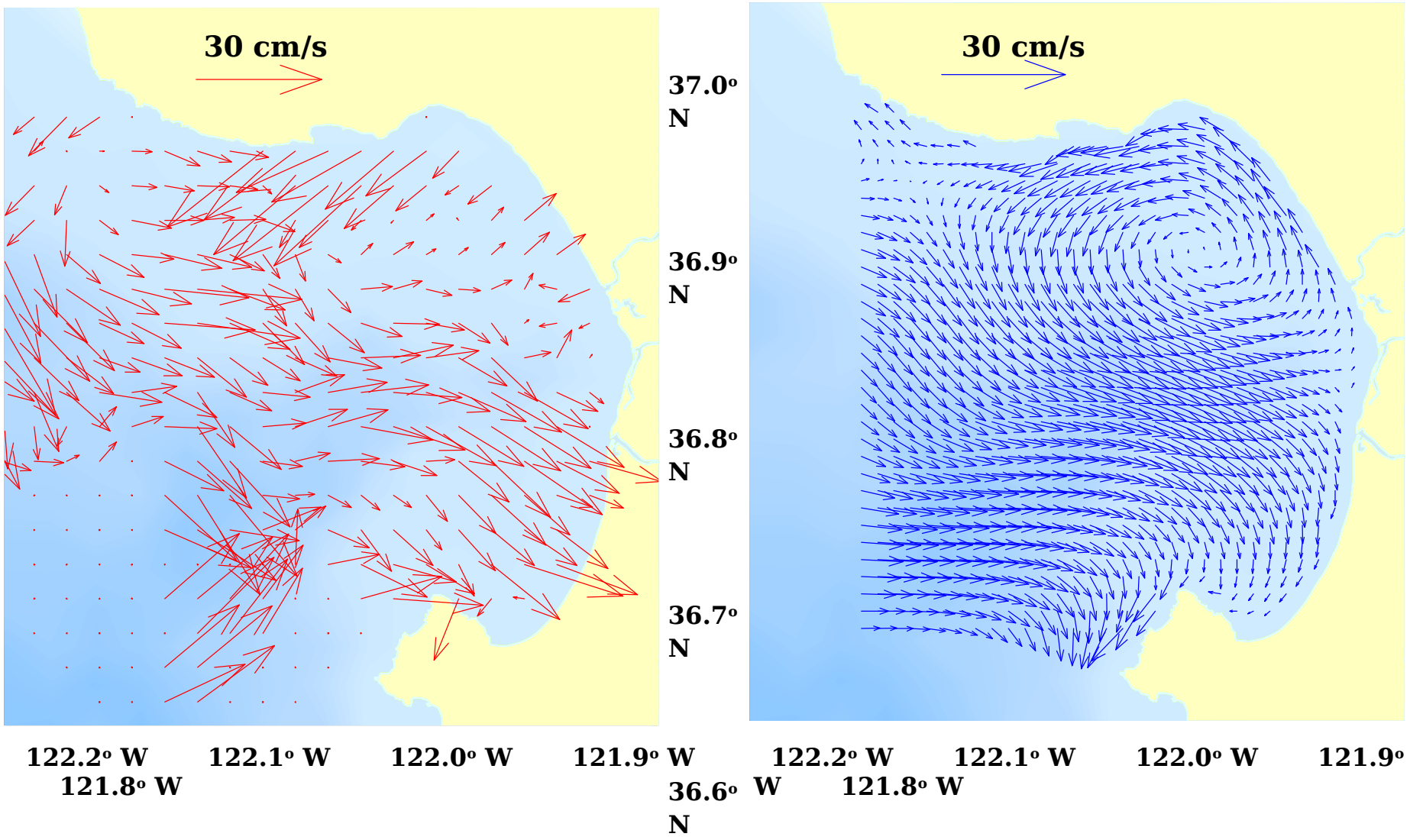

Place for comments: left - radar derived currents for 17:00 UT December 1, 1999

right – reconstructed velocity field.

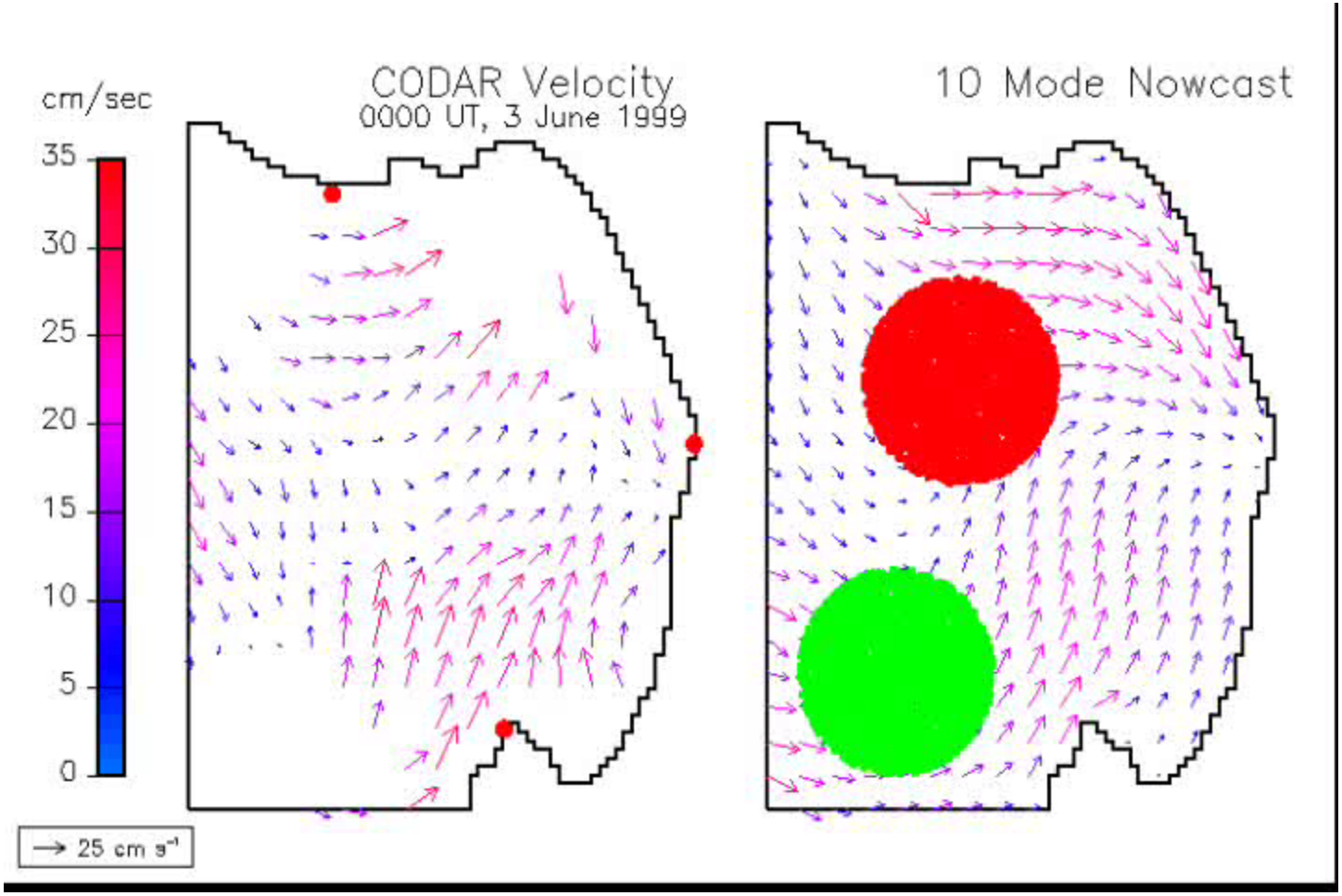
cm/sec
35
30
25
20
15
10
5
0
CODAR Velocity
0000 UT, 3 June 1999
10 Mode Nowcast
→ 25 cm s⁻¹

Conclusions

- OSD is a useful tool for processing real-time velocity data with short duration and limited-area sampling especially the ARGO data.

- OSD has wide application in ocean data assimilation.